CHALMERS
UNIVERSITY OF TECHNOLOGY

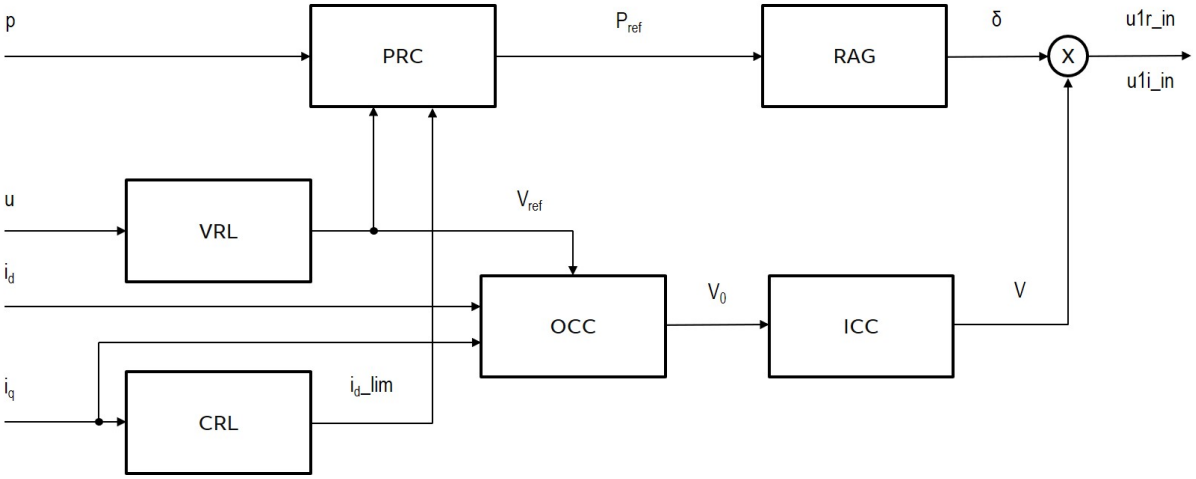

Implementation of Virtual Synchronous Machine to Allow High Penetration of Converter Connected Generation

OBAI BAHWAL

Department of Electrical Engineering
CHALMERS UNIVERSITY OF TECHNOLOGY
Gothenburg, Sweden 2018

Master's thesis 2018:NN

Implementation of Virtual Synchronous Machine to Allow High Penetration of Converter Connected Generation

OBAI BAHWAL

CHALMERS
UNIVERSITY OF TECHNOLOGY

Department of Electrical Engineering
Division of Electric Power Engineering
Chalmers University of Technology
Gothenburg, Sweden 2018

Implementation of Virtual Synchronous Machine to Allow High Penetration of Converter Connected Generation
OBAI BAHWAL

Supervisor: Nicklas Johansson, ABB AB, Corporate Research
Examiner: Massimo Bongiorno, Electrical Engineering

Master's Thesis 2018:NN
Department of Electrical Engineering
Division of Electric Power Engineering
Chalmers University of Technology
SE-412 96 Gothenburg
Telephone +46 31 772 1000

Cover: VSM control model.

Typeset in LaTeX
Gothenburg, Sweden 2018

VSM Implementation
Implementation of Virtual Synchronous Machine to Allow High Penetration of Converter Connected Generation
OBAI BAHWAL
Department of Some Subject or Technology
Chalmers University of Technology

Abstract

Growing demand on producing clean energy and the increasing use of HVDC lines, in power systems, in the recent years, led to magnifying issues that come with it, which were deemed insignificant before. RES and HVDC technologies are interfaced with the grid through converters that does not contribute to the system's inertia, which leads to making the system vulnerable to instabilities. This thesis implements and test converter control as a Virtual Synchronous Machine (VSM) to allow high penetration of converter connected generation. The VSM model is simulated in load step and short circuit events to verify the ability of this technology to emulates synchronous machines and, also, to test the current control functionality of the VSM. The technology proved to be successful in strengthening the system inertia, with the need for more research on more practical test system.

Keywords: VSM, Converter Connected Generation, High Penetration of RES, RoCoF, Inertia Emulation, Swing Equation, Current Control.

Acknowledgements

First and foremost, I thank god for giving the strength in body and mind to finish this master's thesis. Then, I thank my family for pushing forward during the work, even though it was during difficult times.

I am grateful for ABB's Cooperate Research Center for giving me the opportunity to conduct my thesis work with them, under the supervision of Dr. Nicklas Johansson, whom has been a great help in leading throughout the study. I also thank Prof. Lennart Harnefors for his support and advice. I extend my gratitude to Dr. Robert Saers and Mrs. Monika Koerfer for making my work in ABB, Västerås easier. I am thankful for Luqman Arif, a thesis worker at ABB, for tutoring me at the beginning of my work.

I would like to thank Prof. Massimo Bongiorno for being my examiner and his patience with me to finish the work.

I hold my sincere gratitude to ABB Saudi Arabia for supporting me financially throughout the entire master program. Also, for facilitating the thesis opportunity at ABB Västerås.

Obai Bahwal, Gothenburg, September 2018

Contents

List of Figures

List of Tables

List of Abbreviations

NSG	Non-synchronous Generation
CCG	Converter Connected Generation
SG	Synchronous Generation/Generator
GG	Gone Green
VSM	Virtual Synchronous Machine
RES	Renewable Energy Sources
HVDC	High Voltage Direct Current
CCBG	Converter-control Based Generation
DQCI	Direct Quadrature Current Injection
UFLS	Under-frequency Load Shedding
RoCoF	Rate of Change of Frequency
SC	Synchronous Condenser
PI	Proportional-Integral
DSR	Demand Side Response
PLL	Phase Locked Loop
SEBIR	Swing-equation Based Inertial Response
PMU	Phase Measurement Unit
ESS	Energy Storage System

1
Introduction

This chapter provides background motivating the study, objective of the thesis, and the scope of it.

1.1 Background

With the desire to have higher renewable energy penetration in the power grid, it is required to study the implications of such increased penetration. Many countries around the world are already moving towards eliminating synchronous generation [1]. For example, in the United Kingdom, a future energy scenario, called Gone Green (GG), where Non-Synchronous Generation (NSG) reach up to 100% is planned to be running by 2030 [1]. Studies has shown that penetration of NSG, also referred to as converter connected generation (CCG), to more than half of the demand will lead to deteriorated system operation, such as; loss of synchronism or reducing critical clearing time [2]. This is due to connecting renewable energy sources (RES) and other NSG to the grid using converters with complex control schemes, which at such penetration levels will severely impact the stability of the system [1]. Consequently, a number of issues will occur in the different stability classes of a power system, namely; frequency stability, voltage stability, and rotor angle stability [1]. These are usually managed through the inherent parameters of a synchronous machine physical design, whereas, converters may not have these parameters or have them as variables set according to economical consideration for the converter solution [1][2]. Therefore, there is a need for a new converter model to resolve the issues with conventional converters. A paper published by the UK national grid claims that Virtual Synchronous Machines (VSM) have the potential to resolve problems associated with CCG for their GG energy scenario [2].

1.2 Objective

The objective of this thesis is to implement and test VSM control model to address the challenges posed by conventional converter control methodology. Furthermore, the VSM model and the test system will be implemented in PowerFactory and will use RMS studies there to test different system events. Mainly, this thesis will focus on load step events to verify similar or improved frequency response when replacing Synchronous Generators (SG) with VSM. Also, it will test short circuit events to verify the function of the VSM current controller, which assure an feasible converter solution.

1.3 Scope

The thesis work will investigate VSM operation using PowerFactory, a power system simulation tool. Meaning it will not consider the component level of VSM implementation. This is because the aim of this paper is to demonstrate that VSM can allow high penetration of RES and the physical implementation study is a secondary step. Moreover, the study does not include protection schemes, since it can be done in a different study on converter protection and fault detection when NSG is connected. However, the VSM controller will include current controller to limit the converter output current from reaching dangerous levels that could damage the converter.

1.4 Thesis outline

This thesis paper starts by providing background information to motivate the importance of the work and define the objective and scope of work to address the problem. The second chapter explains supporting and background theory to conduct the thesis work. After that, literature review is presented in the third chapter to demonstrate different approaches taken to allow high penetration of CCG. Then, the fourth chapter illustrate how the work is carried to achieve the objective of the thesis. The fifth chapter reports the results obtained by carrying the thesis study with supporting analysis. In the sixth chapter, discussion about the study results and the sustainability aspects of the VSM solution is presented. Finally, the seventh chapter conclude the thesis project and provide recommendation for future work.

2

Supporting Theory [3]

In the following sections, supporting Theory about swing equation and power-angle curve are presented, as well as, system behaviour during load step.

2.1 Swing equation

The resultant torque acting on the rotor of a synchronous machine is given by

$$T_a = T_m - T_e \tag{2.1}$$

where T_a is the accelerating (or decelerating) torque in $[N.m]$, T_m is the mechanical torque in $[N.m]$, and T_e is the electromagnetic torque in $[N.m]$. During unbalance of torques, the prime mover is accelerated proportionally to the inertia of the generator resulting in the equation

$$J\frac{d\omega_m}{dt} = T_a = T_m - T_e \tag{2.2}$$

where J is the moment of inertia of the generator and prime mover in $[kg.m^2]$, ω_m is the angular velocity of the rotor in $[rad/s]$, and t is the time in $[s]$. The kinetic energy stored in the rotor expressed in terms of J and ω_m is

$$W_k = \frac{1}{2}J\omega_m^2 \tag{2.3}$$

where W_k is the kinetic energy in $[W.s]$. The moment of inertia J can be expressed in terms of the per unit inertia constant H as

$$J = \frac{2H}{\omega_m^2}S_{base} \tag{2.4}$$

where S_{base} is the rating of the machine in $[VA]$. Substituting 2.4 in 2.2 results in

$$\frac{2H}{\omega_m^2}S_{base}\frac{d\omega_m}{dt} = T_m - T_e \tag{2.5}$$

which can be represented in per unit as

$$2H\frac{d\omega_r}{dt} = T_m - T_e \tag{2.6}$$

where ω_r is the angular velocity in $[p.u.]$. Since the relationship between power P and torque is given by

$$P = T\omega_r \tag{2.7}$$

and ω_r is assumed to be equal to the synchronous speed, i.e. $\omega_r = 1\ p.u.$, which will result in T and P being equal in per unit; equation 2.6 divided by $2H$ can be written as

$$\frac{d\omega_r}{dt} = \frac{1}{2H}(P_m - P_e). \tag{2.8}$$

The above equation shows that the relation between the rotor acceleration (or deceleration) is inversely proportional to the inertia constant H. Deriving the expression yields the angular position of the rotor in reference to the reference machine in electrical radians, thus, equation 2.8 can be written in terms of swings in rotor angle as

$$\frac{d^2\delta}{dt^2} = \frac{d\omega_r}{dt} = \frac{1}{2H}(P_m - P_e). \tag{2.9}$$

Given that the above equation models the swings of a machine rotor during disturbances, it is referred to as the *Swing equation*.

2.2 Power-angle curve

Consider the following single-machine infinite bus system in its reduced form

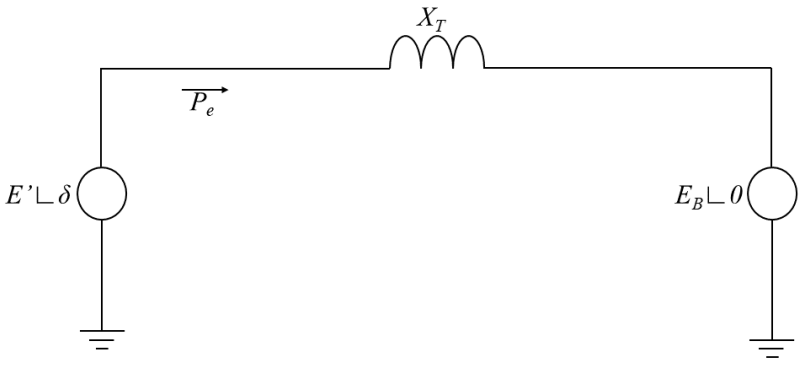

Figure 2.1: Equivalent circuit of a single-machine infinite bus system.

In figure 2.1, E' is the internal voltage of the generator, E_B is the infinite bus voltage, δ is the leading angle of E' with respect to E_B, X_T is the total reactance seen by the generator, and P_e is the electrical power output of the generator, which can be given by the following equation

$$P_e = \frac{E'E_B}{X_T}\sin\delta. \tag{2.10}$$

Using the above equation, P_e with respect to the rotor angle δ can be plotted, figure 2.2, for a given system reactance, and the resultant plot is referred to as the power-angle curve.

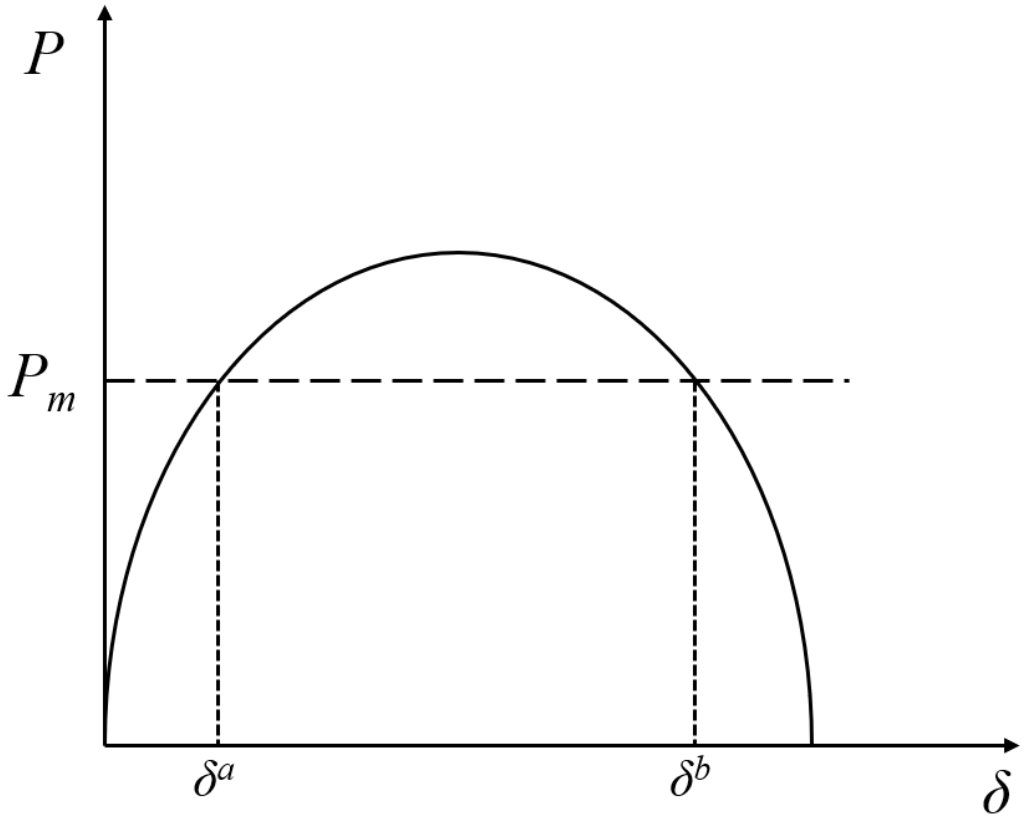

Figure 2.2: Power-angle curve.

where P_m represents the mechanical power input of the generator. Knowing that P_m is equal to P_e during steady-state, it is observed that there are two points in which the equilibrium is satisfied. However, only δ^a will result in a stable system, while δ^b will result of loss of synchronization of the generating unit. Assuming operating point at δ^a; if P_m is increased, by application of equation 2.9, the rotor will accelerate and that will result in advancing the rotor angle of the SG from the reference machine angle. Thus, according to equation 2.10, P_e will increase and a new equilibrium point can be achieved. On the other hand, if the system is operating at δ^b, increasing P_m will lead to an increase in rotor angle, which will result in less P_e. As a result, the rotor will keep accelerating and synchronism between the SG and the grid will be lost.

Using the power-angle curve shown in figure 2.3, SG behaviour during short circuit faults can be demonstrated based on the swing equation 2.9 and equation 2.10. To simplify the analysis, P_m is assumed to be constant during and after the fault. Also, P_e is reduced to zero during the fault and after the fault, it returns to the power-angle curve value based on δ at the fault clearing instant. Initially, the SG is operating

with δ_1, where P_m is equal to P_e. Then, the fault occurs, which will rapidly decrease P_e to zero, leading to accelerating the rotor and gradually advancing the rotor angle to δ_2. After clearing the fault, the power-angle characteristics return to its pre-fault state, resulting in a sudden increase in P_e, which will lead to decelerating the SG rotor. But since the rotor speed is still higher than the grid speed, the rotor angle will keep increasing until the rotor speed reaches the grid speed giving the maximum rotor angle of δ_3. However, the surplus of P_e at δ_3 will result in a further decrease in rotor speed until equilibrium point is reached again. Notice that the speed is now less than the synchronous speed, causing a further decrease of the rotor angle to δ_4. the system will keep oscillating based on the swing equation unless dampers act on the rotor, which will result in stabilizing the system at the initial operating point.

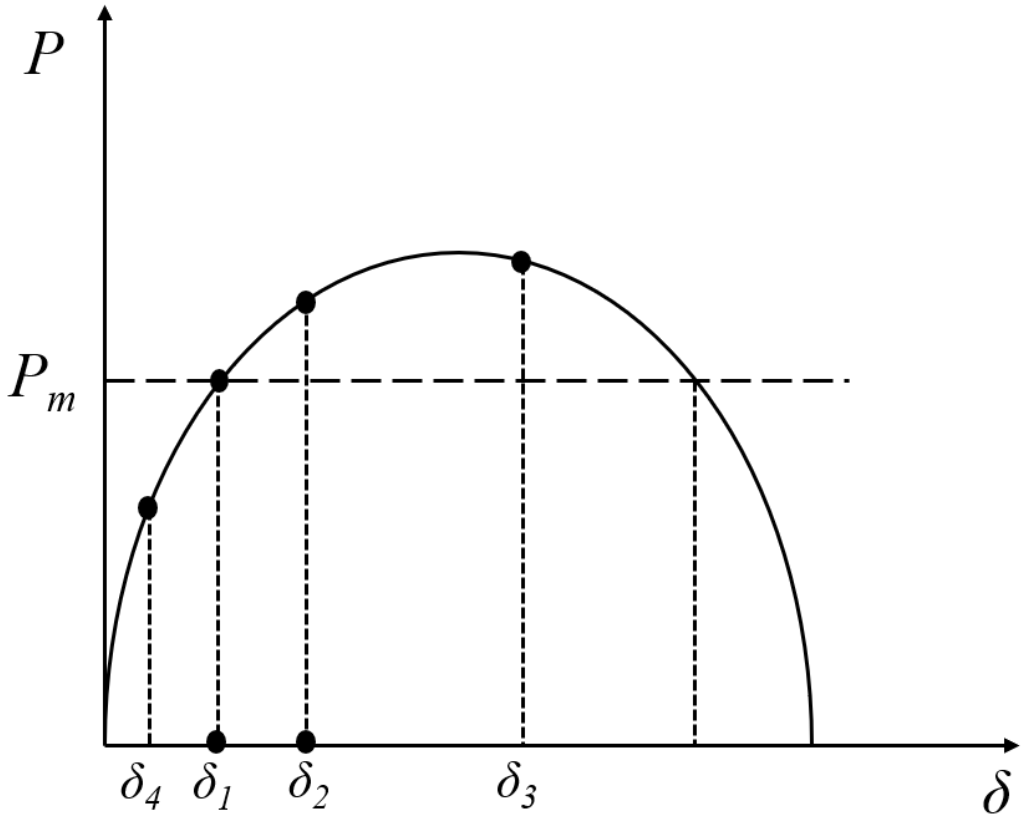

Figure 2.3: SG behaviour during faults.

2.3 System frequency response for a load step

In this section, load step resulting in frequency drop is considered, i.e. increase in load. Following a large frequency imbalance, system frequency go through three different stages. First, inertial response, which decides the RoCoF and the maximum frequency drop (or nadir frequency). This is given by applying equation 2.9 with P_e increased, while P_m remaining constant, and H is the equivalent system inertia.

After that, governing generating units in the system start acting to support the frequency. Governors are machines that are equipped with turbine governors, which makes them able to supply primary reserve power to compensate for the power imbalance, within 30 s of the load step (or generation loss). However, Governors normally allow a certain error in the frequency given by the droop setting R and is given by

$$R = \frac{\Delta f}{\Delta P}. \tag{2.11}$$

This definition entails that a certain percentage change in frequency will result in a 100% change in output power. Finally, frequency is restored to nominal by rescheduling of generating units in the system to balance generation and demand, which is done within 15 minutes from the system event.

3

Literature Review

This chapter provides an introduction to conventional converter control and followed by a summarized review of problems regarding the inclusion of large amount of CCG in the power system. After that, it presents how different system operators and power planners addressed its consequences and gives motivation to adopt the VSM control philosophy.

3.1 Conventional control of CCG

NSG are most commonly connected to the grid through grid-following power converters, where they operate as current sources and have the general structure depicted in figure 3.1 [4][5][6]. Commonly, the converter will be controlled through two cascaded loops, which are an internal current control loop and an external DC-link control loop [5]. Protection against high converter current and mitigating power quality issues is done through the internal current loop, which is characterized with high bandwidth to allow prompt response during system events, by regulating the grid current [4][5]. On the other hand, balancing of the power flow is handled by the DC-link loop [5].

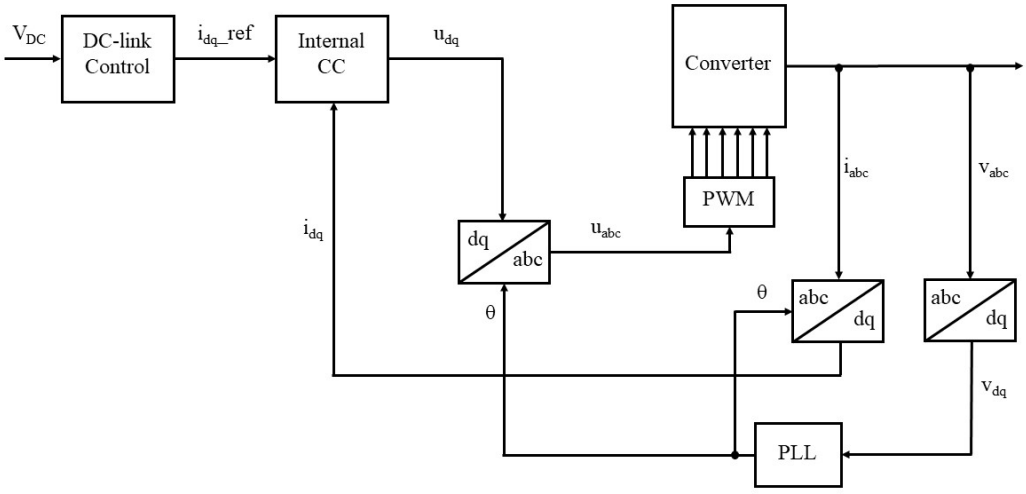

Figure 3.1: Conventional cascaded control structure of CCG.

These converters output three-phase voltages with phase angles extracted from the grid using Phase-Locked Loop (PLL) method [5]. Therefore, grid-following converters need a grid-forming SG, or converter, making an island mode operation not possible otherwise [4]. In the PLL control, the grid voltages and currents are transformed from three-phase to dq-frame, as shown in figure 3.2, where proportional-integral (PI) control is most effective [4][5][6][7].

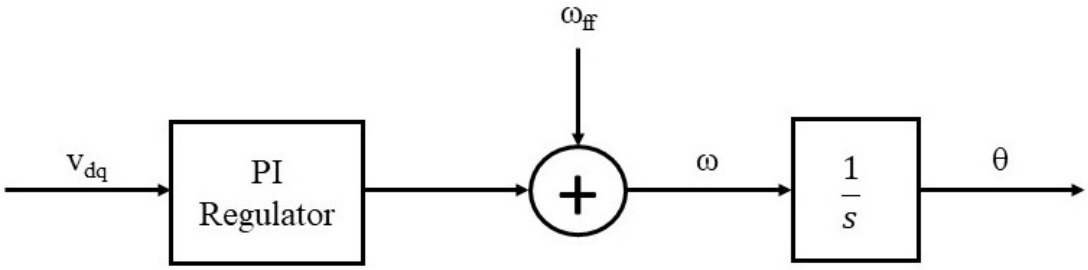

Figure 3.2: General structure of the PLL.

3.2 Effects of increasing CCG

As the vision of many countries around the world aim towards reducing greenhouse emissions, A lot of investments have been made to improve and expand the use of RES [8]. Germany, Ireland, Denmark, and Spain are example of countries that already have a considerable amount RES integrated into their power system [8]. Although that the increased utilization of RES is beneficial from a sustainability point of view, it results in added grid security risks and challenges that otherwise would be avoided in conventional grids [9]. Challenges include; frequency control, voltage stability, rotor angle stability, and active power recovery.

- **Frequency stability:**
  frequency stability is a major concern in a converter dominated system, owing to the fact that the system inertia will reduce significantly [1]. This is due to the absence of rotating mass since the main sources of NSG comes from photovoltaic, HVDC, and wind. While wind has significant rotational mass, it is decoupled using power electronics and HVDC and photovoltaic have no inertial influence, which will lead to similar system behaviour [10]. As a result, the rate of change of frequency (RoCoF) will increase, leading to lower nadir frequency [1]. Hence, it is required to address the system inertia reduction and its consequences to avoid frequency instability.

- **Voltage stability:**
  In a system with the majority of generation being converter connected, voltage support during faulty conditions will prove to be challenging. That is because converters output current needs to be limited in order to obtain an economically viable converter solution [2]. In addition, protection may not operate or malfunction, given the low levels of fault current contribution [2].

- **Rotor angle stability:**
  In power systems where converter control-based generation (CCBG) is present, SG and CCBG interact dynamically [11]. This interaction is, normally, small, when the penetration level of CCG is low [11]. However, once the penetration level gets higher, the impact of the dynamic interaction is significant and that will greatly affect the small-signal angular stability [11]. Direct Quadrature Current Injection (DQCI) is the converter type used for NSG, which have normally control bandwidth of more than 100 Hz [2]. To model a complete system and study the synchronous interaction between machines and converters at that frequency level, and when NSG is dominant, is not feasible [2]. Furthermore, having higher penetration of CCG will lead to an increase in rotor angle deviation for SG and settling time, following a system contingency, which will be more significant when NSG replaces SG [12]. Therefore, a new converter control technique needs to be investigated to connect NSG to the grid [2].

- **Active power recovery:**
  Wind is one of the major RES being integrated into power systems. However, wind turbine generators recover active power slowly compared to SG, with response time between 1-4 s, after short-circuit faults [10]. This slow recovery could lead to alarming frequency stability issues depending on the location of the wind farm [10].

3.3 Suggested solutions

Primary control is used in power systems to prevent frequency from reaching low level, i.e. 49 Hz as per European practice, following a disturbance to prevent more extreme measures like under-frequency load shedding (UFLS) [13]. That is done by fully activating primary reserve within 30 s from the disturbance [13]. A study shows that systems with large penetration of wind should utilize wind turbines as primary reserve, along with SG, and that should decrease the RoCoF. However, it is noted that using wind turbines as primary reserve might be an expensive solution, since they will have to operate at less than their optimum rating, and requires further research [13].

Another solution suggested for Great Britain's (GB) system operator is to raise the limits for tripping relays that senses RoCoF and calibrate it so that it secure the

system from the larger loss of generation or demand in a given grid [14]. Alternatively, Synchronous Condensers (SC) have the potential to boost the system inertia, which in turn will reduce the RoCoF [14]. SC is arguably an economic solution especially for systems where NSG displaces SG; that is because displaced SG could be transformed into SC and save construction costs, however further studies needs to be considered to verify the effectiveness of this solution [15].

Other solutions include Demand Side Response (DSR) management and energy storage [14]. with proper communication between consumers and suppliers and data management, DSR could be a feasible solution to address imbalance of generation and load, where consumers reduce their power consumption to compensate for lack of generation [14]. Moreover, different energy storage technologies could be used to store energy during peak production times and deploy it during low production times in no more than a second [14]. Thus, energy storage is viable countermeasure against the increase of RoCoF in low inertia power systems [14].

Virtual Synchronous Machine (VSM) is a widely emerging term in the research field and vouched for as a promising solution for future power grids. In 2007, the leading publication regarding VSM was presented to address new energy policies, including displacing conventional generation with RES and moving towards decentralized energy generation [16]. VSM is a control scheme for converters that make them behave, partly or fully, like a synchronous machine, depending on the implementation [2]. [17] presents one of the initial models for VSM implementation where an inertia emulation outer loop provides required references for the controller. But due to the interaction caused by the cascaded control structure, an eigenvalues-sensitivity based tuning technique was developed to maintain the controller effective operation [17]. However, the model does not provide primary frequency control or consider grid dynamics since it mainly tunes control parameters [17][18]. Alternatively, other control methods that rely on PLL to sense voltage angle were reviewed in [19]. The review explains that such methods do not deliver the capabilities expected from the VSM concept since they would still require inertial presence in the grid [18][19]. There are many examples found in literature and some of them are presented briefly in the following.

- **SEBIR control:**
  The Swing-Equation Based Inertial Response (SEBIR) method compensate with active power in case of power imbalance in the system [20]. While it uses frequency measurement in order to determine the active power compensation needed, it does not use PLL techniques to measure frequency [20]. Instead, Phase Measurement Units (PMU) of class P and M are employed, where frequency is measured through symmetric filters over 3 and 11 cycles respectively [20]. It is important to note that SEBIR control method only adds an additional control loop, with PMU and inertia constant, to existing DQCI converter schemes, meaning that the converter ultimately acts as balanced sinusoidal current source [20]. Contrary to expectation, SEBIR proved

to decrease the penetration level of NSG to a power system before it loses stability [20]. This is due to the slow frequency measurement that leads to slower injection of active power to support the system. Also, the dynamics of the DQCI controller still exist, since the DQCI is only equipped with SEBIR, which leads to unpredictable interaction between the control loops [20].

- **VISMA:**
  Another approach is VISMA, which also refers to virtual synchronous machines, however, this inverter control represents a synchronous machines control by calculating different current references [21]. While VISMA is considered a current source, similar to SEBIR, it is a standalone inverter control mimicking a synchronous machine. The controller has embedded virtual torque and virtual excitation that are used for active and reactive power regulation [21]. In addition, Inertial response, along with virtual damping, is setup in the control to improve the frequency and power profile during disturbances, similar to SG [21]. VISMA control strategy is simulated in a micro grid and proven to exhibit the aforementioned properties [21].

- **VSM0H converter:**
  Virtual Synchronous Machine Zero Inertia (VSM0H) converter model works as a voltage source similar to SG, however, the controller does not have an inertia constant implemented [20]. The only necessary measurement needed as input is the output current from the converter [20]. The model derives its voltage phase angle from an integrator and it does not aim to produce a balanced sinusoidal current through inner current control [20]. Due to the absence of synthetic inertia in the controller, the VSM0H would lead to a rapid change of frequency, to the new system frequency, after an active power disturbance [20]. Thus, VSM0H control strategy does not decrease RoCoF, but it helps preventing frequency from reaching UFLS level. It has been shown that this method allows up to 100% penetration of NSG while maintaining a stable system [20].

- **VSM converter:**
  Although results from using VSM0H were promising, there is still the issue with RoCoF when there is a significant generation to load disturbance, due to the lack of inertial response from the converter [22]. Hence, further studies were carried out to obtain a dynamic converter behaviour similar to synchronous machines by emulating inertia in its control [22]. It is argued that VSM might have better performance compared to SG, since undesirable SG characteristics could be disregarded in the control scheme of VSM [22]. Similarly, SG also might outperform VSM in certain aspects depending on the converter design limits like the maximum fault current allowed [22]. The control strategy is similar to that of VSM0H, but with added inertia. Using the converter voltage and current in the dq-frame, instantaneous power is computed and subtracted from the reference [22]. The difference is passed through an integrator where

the inertia constant applied to obtain slip speed. By integrating the slip, the virtual rotor angle is obtained [22]. The controller outputs a phasor voltage consisting of a reference voltage magnitude and the virtual rotor angle [22]. This means that during system events the only control signal affected is the virtual rotor Angle, assuming no droop control on the voltage reference. Dynamic breaking is an additional control block after the power difference and before the inertia emulation, which stops the virtual rotor angle from increasing in case of nearby short circuit faults [22].

- **ST-VSM**
  Providing inertial response entails injecting power to the grid during transient events to stabilize the frequency [23]. For instance, in case of loss of generation, the frequency will start to decrease until it reaches a minimum value depending on the inertia constant [23]. Then, the frequency will start to increase and oscillate until it reaches steady state and the stabilizing time depends on the damping power injection [23]. Self-Tuning Virtual Synchronous Machine (ST-VSM) is an approach that aims to vary inertia and damping constants, which are constants in SG, during Converter operation [23]. This is done with the objective of reducing frequency transients and power injection from the converter's Energy Storage System (ESS) [23]. The control philosophy of ST-VSM is that it searches for optimal inertia and damping constant during frequency deviation, which are adjusted after every control cycle, but it only tunes damping constant during normal operation while setting the inertia constant to zero [23]. Positive results were achieved when applying this method in simulation, where a reduction of 58% energy injection from ESS was reached [23]. However, load type may result in greater energy requirement from the ESS when adopting ST-VSM compared to constant parameters VSM [23].

3.4 Motivation to use VSM control

Given the precedent review, there are several points where the VSM technique has the edge over the conventional cascaded control of converters in high penetration levels. First, conventional control leads to an increased RoCoF, due to the absence of inertia response, while VSM helps with RoCoF, by providing inertial response [2][22]. Second, since cascaded control relies on PLL to obtain the voltage angle from the grid, then at high inclusion CCG there is a risk of losing synchronizing power and reference voltage [2][5][22]. Whereas the VSM uses a pure integral control to derive the voltage angle, thus, it can provide reference voltage and synchronizing power, similar to SG [2][22]. Third, Contrary to the cascaded control, which require a high bandwidth to guarantee fast controller response, the VSM can operate on a limited bandwidth, which will reduce the risk of high frequency instabilities [2][5][4][22]. Also, the limited bandwidth of VSM control would reduce the sensitivity to load imbalance and harmonics expected when using DQCI control, because it will lead to absorbing the unbalanced currents to some extent[2][22]. However, further studies are needed to confirm that limiting the control signals' bandwidth would help when

absorbing voltage unbalance, since that would require a larger capacitor and could lead to power modulation in the converter's DC side [22]. Fourth, Although the VSM is constrained by the current limits of the converter's switching devices, like any common converter, it provides a fault current in-feeds (balanced or unbalanced) within 1 control cycle at any power factor. This is faster than conventional control and can help with fault detection and tackles protection operation challenges when using CCG [2][22]. Fifth, the VSM naturally delivers reactive power during faults, to support the voltage that clears away after the fault. This helps with mitigating voltage instability issues faced with cascaded control, which usually do not deliver any output during faults [2][22].

4

Methods

The methodology used to conduct the thesis work is explained in this chapter.

4.1 VSM control

The VSM control is based on direct realization of the swing equation with the power measurement, at the connected bus, as the only essential input control signal and the output signals being the real and imaginary voltage settings of the converter. In addition, power reference P_{ref} and voltage reference V_{ref} are required signals for the control, while, frequency, voltage, and reactive power measurement could be used to create power and voltage references based on droop settings. In the VSM implementation used, P_{ref} is the power settings of the converter and V_{ref} is obtained by passing the difference of the measured bus voltage and the voltage settings of the converter through a PI controller.

The simple VSM control that was used for the initial study is shown in figure 4.1. First, the measured power is subtracted from the reference power, representing $(P_m - P_e)$ in equation 2.9, in per unit. Then, the difference is multiplied by the inertia constant in the swing equation, i.e. $1/2H$, and integrated to obtain the speed deviation, or the slip speed, from the nominal. After that, the slip is integrated to get the virtual rotor angle in per unit, which is then multiplied by 2π to obtain it in radians. The slip is also fed back through a washout filter and subtracted from the reference power. The feedback will act as an active damping that will work only during power imbalance. Finally, the reference voltage is multiplied by the cosine and sine of the virtual rotor angle to create the real and imaginary voltage output signals. This simple implementation was used to verify the emulation of a synchronous machine.

However, it was observed that during load step events there is almost no energy delivered from the VSM. This contradicts equation 2.3 in the event where the settling frequency is lower than the initial, nominal. To remedy that, another feedback, KG was implemented in which the slip speed in multiplied by a constant and subtracted from the reference power. The value of KG is proportional to H and can be tuned to control the contribution of the VSM to the grid stability.

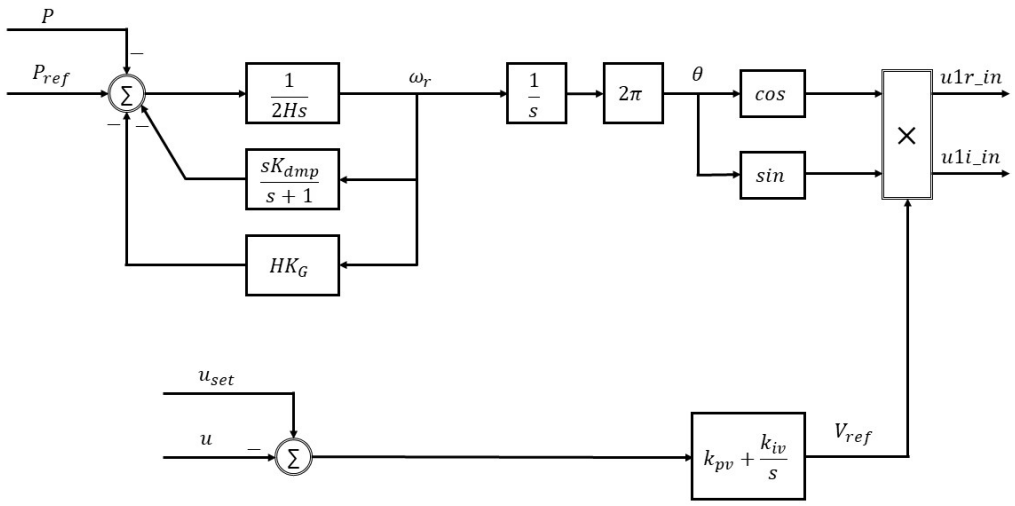

Figure 4.1: Basic VSM control.

A more elaborate implementation was constructed to realize a safe operation of a converter. The improved model includes; voltage reference limiter (VRL), current reference limiter (CRL), power reference control (PRC), outer current control (OCC), inner current control (ICC), and rotor angle generator (RAG). The control block diagram is show in figure 4.2.

- **VRL:**
  The voltage reference control aims to limit the reference voltage V_{ref} during severe grid voltage depression. V_{ref} is obtained by implementing the relation

$$V_{ref} = (V_{nom} - V_{PCC})(k_{pv} + \frac{k_{iv}}{s}), \tag{4.1}$$

  where V_{nom} is the nominal voltage setting, V_{PCC} is the measured voltage at the point of common coupling, and k_{pv} and k_{iv} are proportional and integral constant respectively, which . k_{pv} and k_{iv} are set to 1 and the PI controller is used to derive V_{ref} for the purpose of initialization in PowerFactory. That is because simply setting V_{ref} to 1 $p.u.$ could result in static error in RMS simulations in the case the controller voltage is different from the converter voltage resulting from the power flow solution. Furthermore, V_{ref} has a dynamic upper limit that is reduced in the case of grid voltage depression.

- **CRL [24]:**
  the purpose of this controller is to reduce i_d current, by prioritizing i_q current, during faults. The output of this control block is a limited current, i_d^{lim}, that is used to limit P_{ref} in the basic control scheme. This is done by setting

$$i_d^{lim} = \sqrt{I_{max}^2 - i_q^2}, \tag{4.2}$$

where i_q is limited by I_{max} and I_{max} is the maximum allowed current.

- **PRC:**
  Here, the reference power is modified based on the output from the VRL and the CRL blocks. P_{ref} is obtained by first dividing the converter power setting by V_{ref}. the signal obtained represent a reference current that is limited by i_d^{lim}, which is then multiplied by V_{ref} to get P_{ref}. Notice that during severe fault conditions, V_{ref} will be reduced and i_d^{lim} will be close to 0, resulting in a reduction in the reference power that will be used to generate the virtual rotor angle.

- **OCC:**
  Resonators can be added in the outer current control for harmonics and negative-sequence control. The resonators are needed for practical implementation and were not required in the simulations, hence, there were omitted from the controller.

- **ICC:**
  The inner current control acts during system faults, when the converter's output current exceed 1 *p.u.*, i.e. it will saturate the output current of the converter to 1 *p.u.*. V_0, which is the input to ICC, is subtracted from the measured output converter voltage, then, divided by a virtual impedance $R_i = 2$ to obtain a current signal. Then, the current is summed with the converter's i_{dq} and passed through a saturation block in which the saturation value is set to 1 *p.u.*. After that, the current is subtracted from i_{dq} and multiplied by R_i to be added to the measured output voltage of the converter once again to obtain V. It can be noted that during steady state, the ICC will have no effect, i.e. $V_0 = V$, but during system faults $V_0 > V$.

- **RAG:**
  It generates the virtual rotor angle in a similar manner to figure 4.1, i.e. the following equation is implemented;

$$\Delta\omega = \frac{d\delta}{dt} = \frac{P_{ref} - p}{2H}(\frac{1}{s}) - D, \tag{4.3}$$

  where D is given by

$$D = \Delta\omega(\frac{sK_{dmp}}{1+s} + K_G H). \tag{4.4}$$

  In the above relations, $\Delta\omega$ is the virtual speed deviation from the nominal speed, K_{dmp} is the damping coefficient, and K_G is a droop coefficient. The parameters are set as follow:
  - H is varied between 3, 5, and 7 during the study to observe the effects of different inertia constants.
  - K_{dmp} is set to 50 as it was found to be suitable to obtain well-damped signals for the simulations, but can be set differently as long as it is not

lower 10, since that could lead to sustained oscillations in the system or it will take a long time to stabilize.

– K_G is set through trial and error to the value 0.003.

Note that the second term in (4.4) was found to have significant impact on improving the frequency response during load to generation imbalance. Finally, the virtual rotor angle is given as

$$\delta = \Delta\omega \frac{1}{s}. \tag{4.5}$$

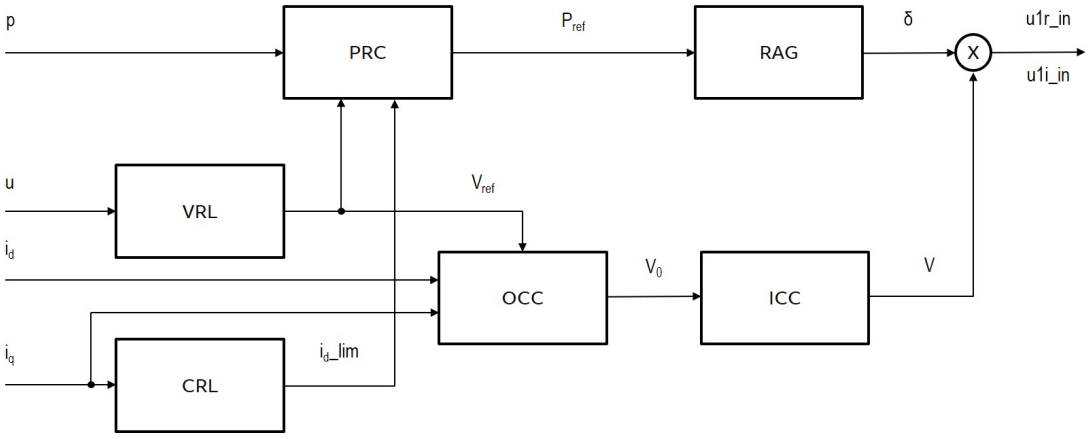

Figure 4.2: Block diagram of improved VSM control.

4.2 Test system

In order to conduct the thesis study, a simple 3-bus test system was built and different test scenarios were simulated using PowerFactory's RMS simulation. The system consists of a SG with hydro governor connected at the slack bus -Terminal(4)-, a constant power load connected at the PQ bus -Terminal(3)-, and a static generator and a SG connected at the PV bus -Terminal-. Moreover, the slack bus and the PV bus are connected to the load through a 50 km lines, which have a model taken from the industry to simulate real lines. To represent CCG, the static generator was used and the VSM control model was implemented in it, hence, it will be referred to as VSM for the remaining of this report. Furthermore, the VSM and SG, at the PV bus, has similar ratings and were used alternatively for comparison in different test scenarios. The system schematics and specifications are shown in figure 4.3 and table 4.1 respectively. Note that the SG_{ref} is connected to the system without a transformer, hence, the unconventional V_{rated} of the machine (110 kV). This is done because the addition of a transformer will basically adds an additional impedance after the SG_{ref} and will not impact the main purpose of the study.

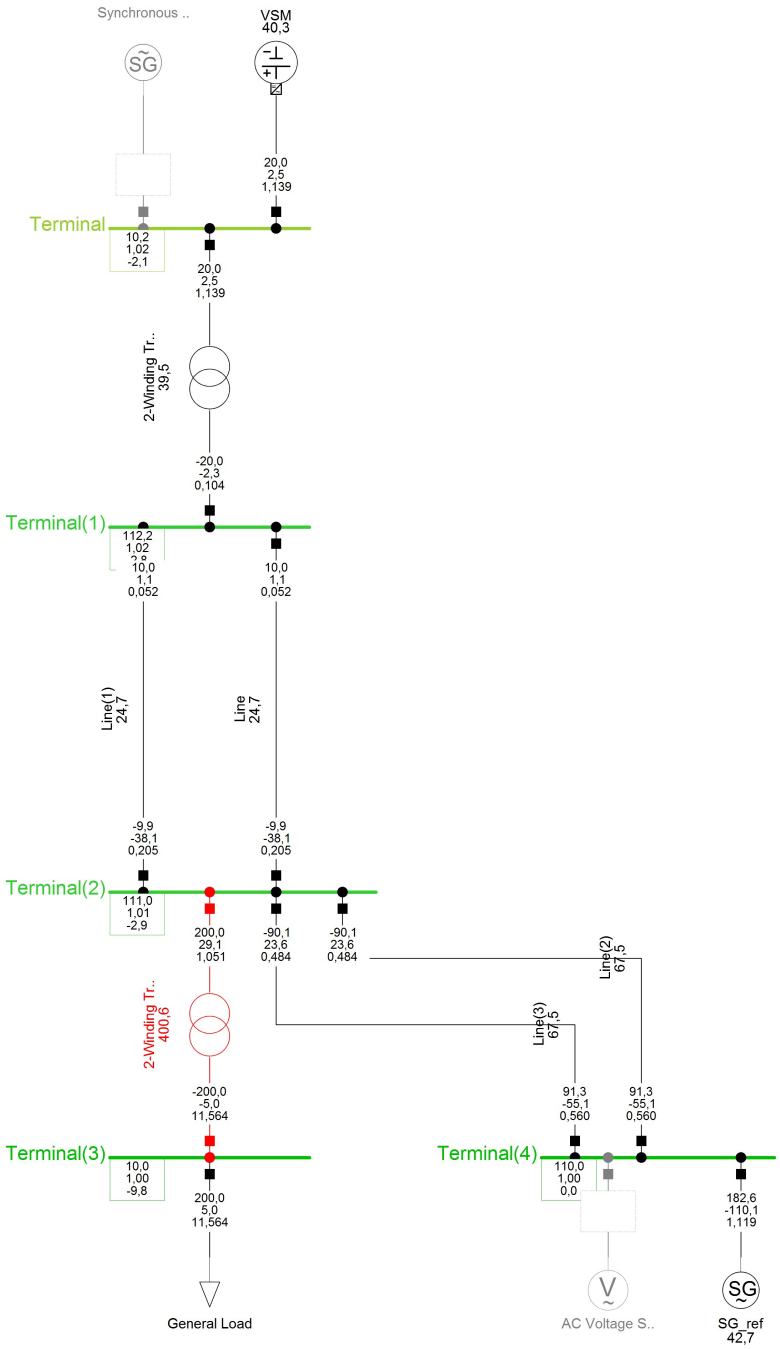

Figure 4.3: Test system used in simulations.

Table 4.1: System settings.

Element	V_{rated} (kV)	S_{rated} (MVA)	P (MW)	Q $(MVAr)$	X_{ss} $(p.u.)$
SG_{ref}	110	500			0.3
SG	10	50	20	2.5	0.3
VSM	10	50	20	2.5	0.3
$Load$	10		200	5	

4.3 Load step (case study 1)

One of the main purposes of this research is to obtain a similar or improved frequency profile, after a power imbalance, when there is high inclusion of CCG compared to SG dominated power system. To test that, a load increase of 25% was simulated in three different scenarios. First, only the governor machine is connected while the SG and the VSM are out of service. Second, the governor and the SG are feeding the load while the VSM is disconnected. Third, the VSM is in service while the SG is disconnected. In the later two scenarios, the inertia constant is varied, for the SG, and the VSM, between 3 s, 5 s, and 7 s to see the effect of inertia on the frequency response and wither it will have different response from SG. The load step study is conducted twice; initially, on the basic swing equation-based control, then, on the improved version with current controller included. This is to investigate how the current controller would affect the emulation of the synchronous machine.

4.4 Short circuit (case study 2)

The VSM is limited to what the converter can withstand, i.e. the current output should not exceed the converter current limit, hence, it is important to simulate extreme system conditions where high fault currents are expected. To achieve that, a close by, at terminal(1), and far away, at terminal(2), short circuit faults were carried on both the simple control and advanced control with a fault duration of 250 ms. Similar to load step events, the inertia constant was varied while connected either the VSM or the SG and compared with each other. First, the test was run on the basic control to confirm SG-like behavior during faults. After that, the improved control was tested to verify current limitation to 1 p.u.. Also, a time constant of 0.003 s was used for slip speed integrator to obtain faster control action during the short circuit fault, since it was observed that the controller will take too long to stabilize the virtual rotor angle.

5

Results

The results from the load step and short circuit simulation are presented in the following sections in two different cases; VSM without current control and VSM with current control.

5.1 Case study 1

5.1.1 VSM without current control

The simulations presented here illustrate the basic control behaviour of the VSM during load increase of 25% and compare it to a SG with similar ratings and parameters. Figures 5.1, 5.2, 5.3, and 5.4 show the voltage, active power, reactive power, and frequency, at the connected bus, respectively, for $H = 3\ s$, $H = 5\ s$, and $H = 7\ s$. Note that the frequency plot has the frequency when there is no machine connected at 'Terminal' in figure 4.3. It is observed that voltage, reactive power, and frequency exhibit similar characteristics when compared to the SG, with the VSM having a slightly better performance. However, for the active power results, it is assumed that the reason for difference in the signal is due to the controller of the SG, since the oscillations seen from the VSM are what is expected based on the swing equation.

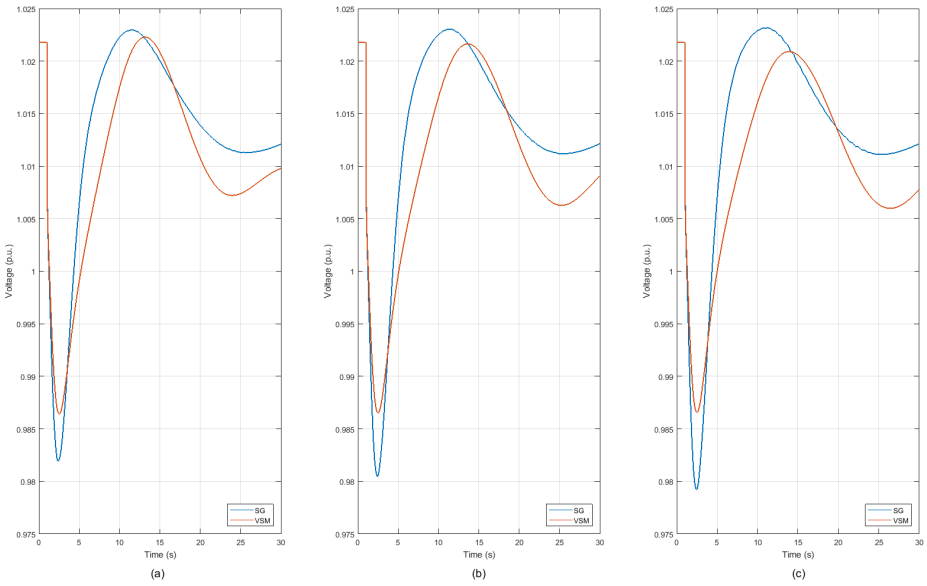

Figure 5.1: The voltage output of the VSM and SG during load step, when using the basic control on the VSM, for different values of H (a) $H = 3\ s$, (b) $H = 5\ s$, and (c) $H = 7\ s$.

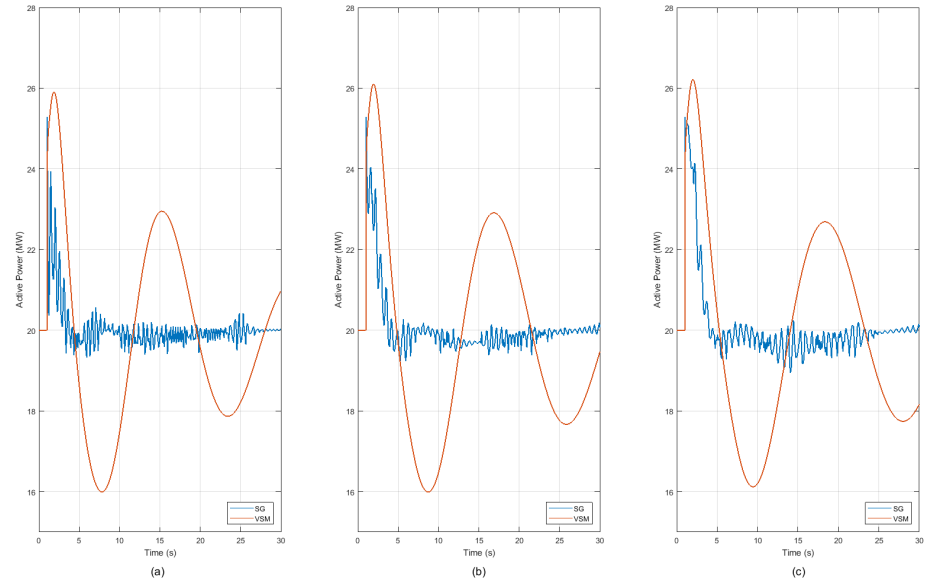

Figure 5.2: The active power output of the VSM and SG during load step, when using the basic control on the VSM, for different values of H (a) $H = 3\ s$, (b) $H = 5\ s$, and (c) $H = 7\ s$.

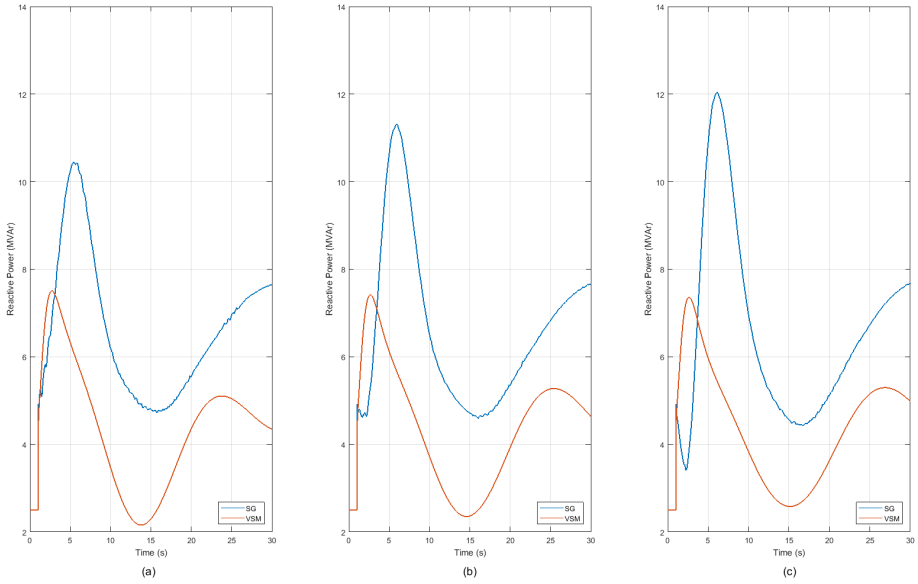

Figure 5.3: The reactive power output of the VSM and SG during load step, when using the basic control on the VSM, for different values of H (a) $H = 3\ s$, (b) $H = 5\ s$, and (c) $H = 7\ s$.

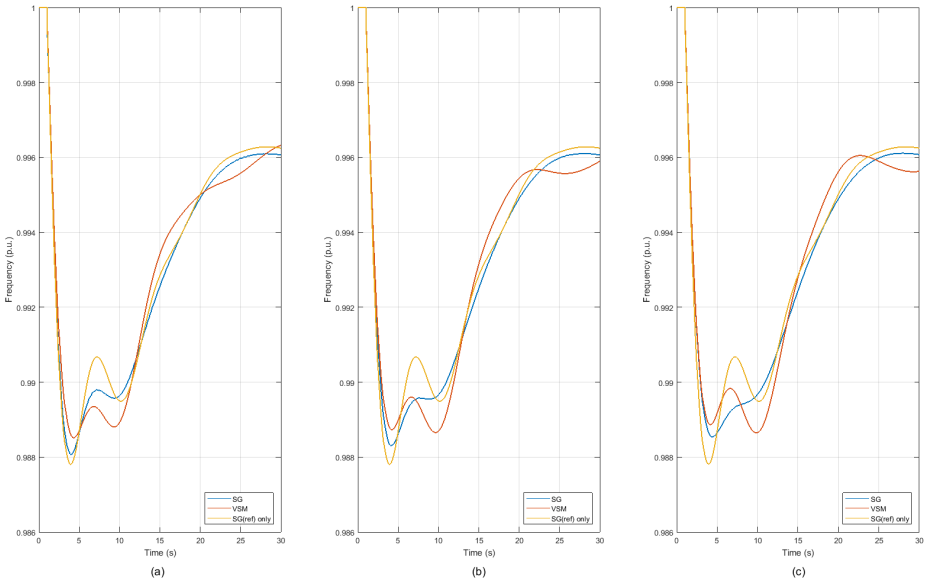

Figure 5.4: The frequency at the bus where the VSM and SG are connected during load step, when using the basic control on the VSM, for different values of H (a) $H = 3\ s$, (b) $H = 5\ s$, and (c) $H = 7\ s$.

5.1.2 VSM with current control

Similar signals were considered when implementing the current control in the VSM, i.e. voltage, active power, reactive power, and frequency, which are shown in figures 5.5, 5.6, 5.7, and 5.8. In general, the current control implementation did not affect the behaviour of the VSM during the load step. However looking at the reactive power plots and comparing it to figure 5.3, it is noticed that there is some changes in the VSM signal resulted from the current controller. That is because the current control acts during system transients and prioritize reactive currents; which led to the changes seen in the reactive power plots. While the difference in signals is minor, it is expected to observe different behaviour duo to the added control loops for current control.

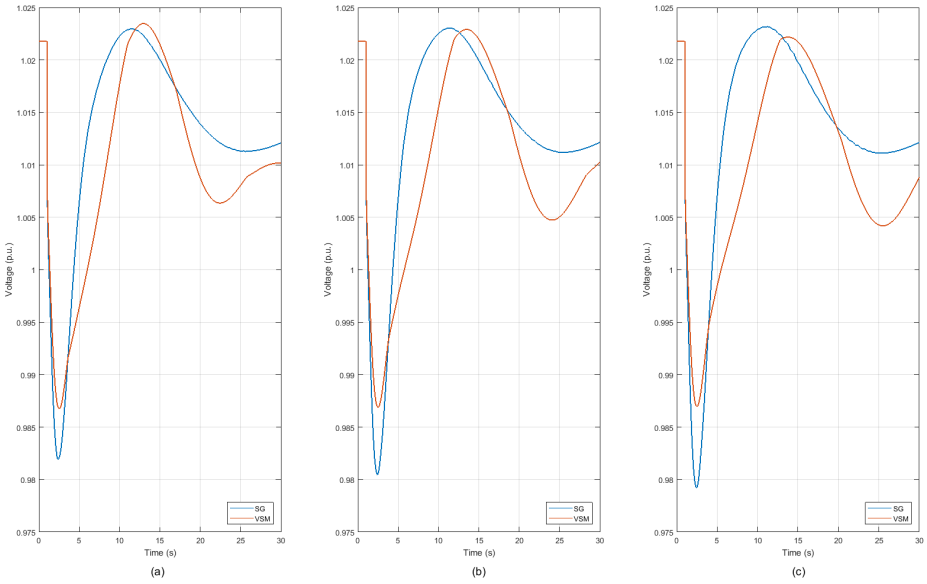

Figure 5.5: The voltage output of the VSM and SG during load step, when using the improved control on the VSM, for different values of H (a) $H = 3\ s$, (b) $H = 5\ s$, and (c) $H = 7\ s$.

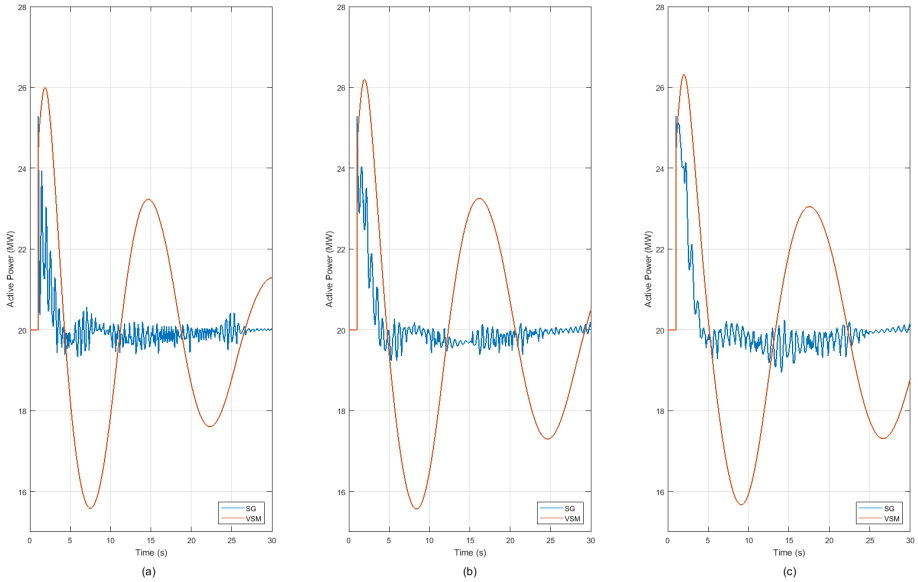

Figure 5.6: The active power output of the VSM and SG during load step, when using the improved control on the VSM, for different values of H (a) $H = 3\ s$, (b) $H = 5\ s$, and (c) $H = 7\ s$.

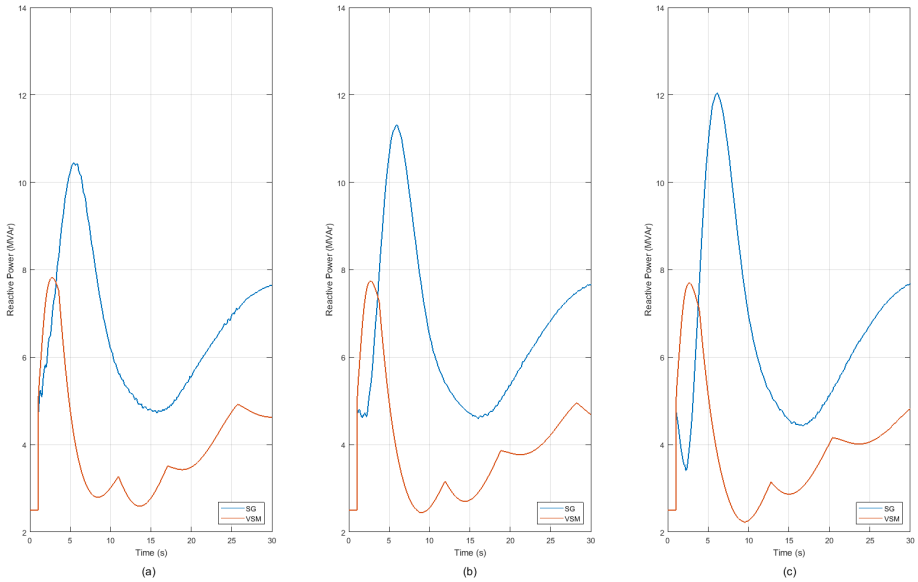

Figure 5.7: The reactive power output of the VSM and SG during load step, when using the improved control on the VSM, for different values of H (a) $H = 3\ s$, (b) $H = 5\ s$, and (c) $H = 7\ s$.

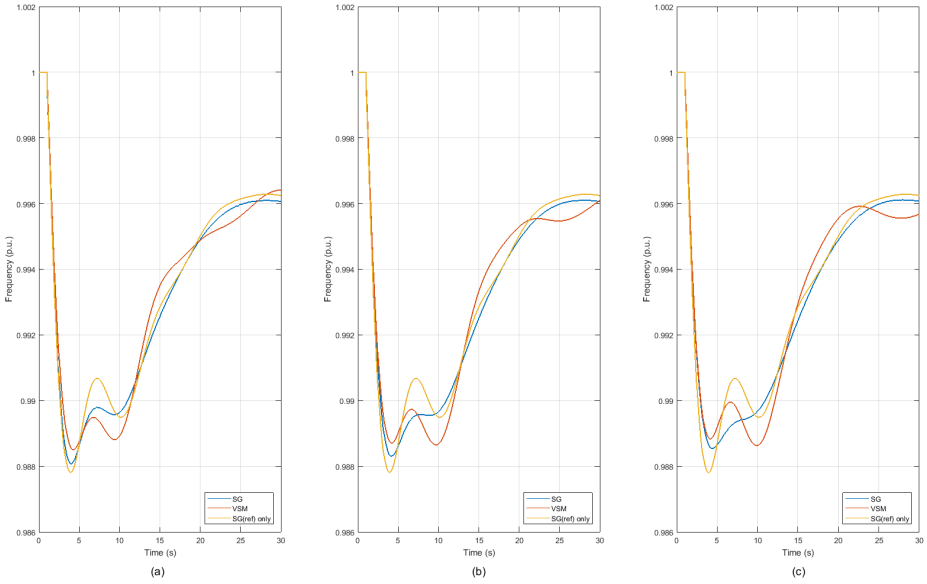

Figure 5.8: The frequency at the bus where the VSM and SG are connected during load step, when using the improved control on the VSM, for different values of H (a) $H = 3\ s$, (b) $H = 5\ s$, and (c) $H = 7\ s$.

5.2 Case study 2

5.2.1 VSM without current control

In this case study, the VSM is tested when applying a balanced 3-phase short circuit fault, for 250 ms, at 'Terminal(1)' and 'Terminal(2)' in figure 4.3. Moreover, the SG and VSM were tested against an AC voltage source as the reference machine, to represent an infinite bus. This is done to avoid interactions from the governing machine and compare the VSM to SG in a simplified system. Six signals are considered for short circuit study; voltage, current, active power, reactive power, rotor speed, and rotor angle. The study results for different H values are presented in figures 5.9, 5.10, 5.11, 5.12, 5.13, and 5.14. The signals presented greatly match the SG signals, with the VSM having more oscillations resulted from using low damping coefficient in the basic control structure. It is important to note that the rotor speed and rotor angle plots for VSM are taken by plotting wr and $rad\text{-}pu$, respectively, from the controller in figure 4.1, which are control signal representing the virtual rotor speed and virtual rotor angle. Also, the signal wr is the virtual slip speed, as mentioned in section 4.1, thus, 1 $p.u.$ is added to the signal in order to compare it to the SG rotor speed.

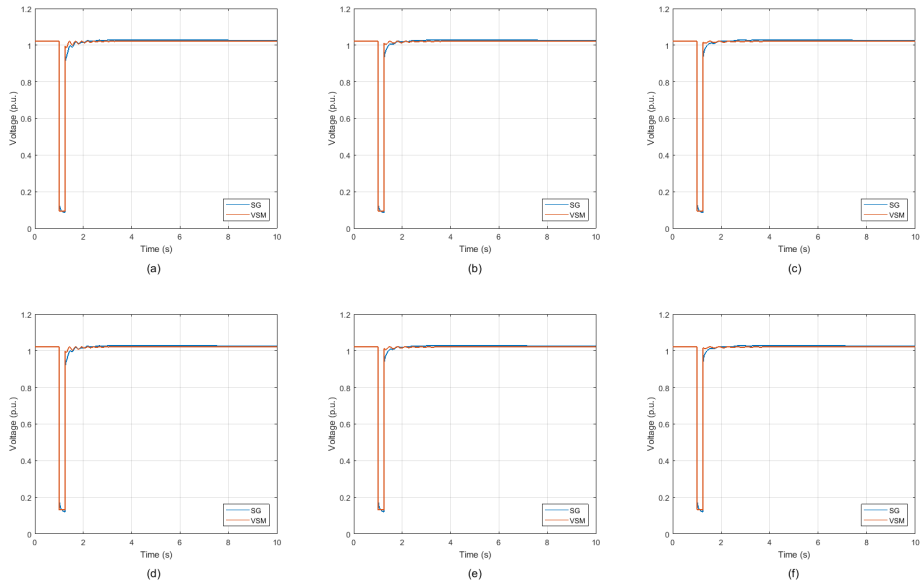

Figure 5.9: The voltage output of the VSM and SG during short circuit, when using the basic control on the VSM, for different values of H (a)(d) $H = 3\ s$, (b)(e) $H = 5\ s$, and (c)(f) $H = 7\ s$. (a),(b), and (c) show results when applying short circuit at 'Terminal(1)' and (d),(e), and (f) show results when applying short circuit at 'Terminal(2)'.

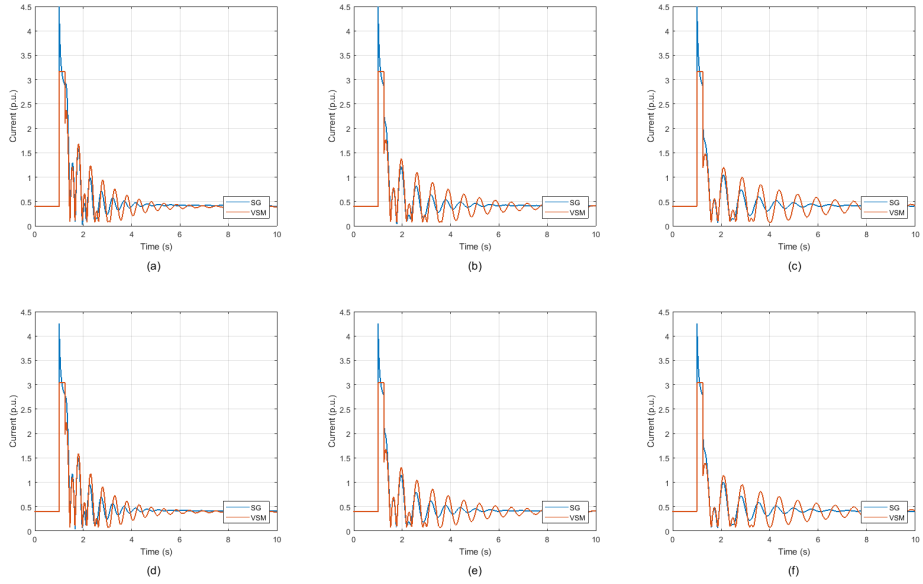

Figure 5.10: The current output of the VSM and SG during short circuit, when using the basic control on the VSM, for different values of H (a)(d) $H = 3\ s$, (b)(e) $H = 5\ s$, and (c)(f) $H = 7\ s$. (a),(b), and (c) show results when applying short circuit at 'Terminal(1)' and (d),(e), and (f) show results when applying short circuit at 'Terminal(2)'.

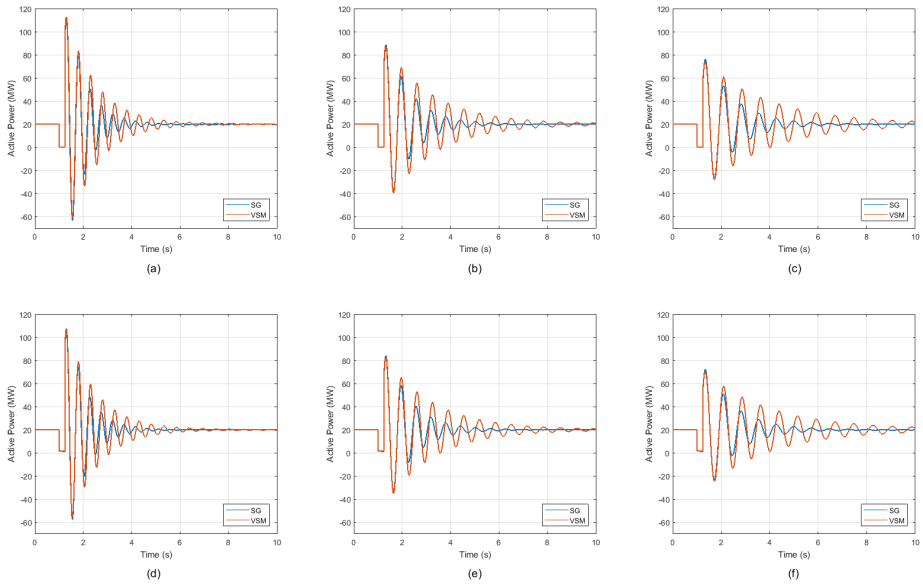

Figure 5.11: The active power output of the VSM and SG during short circuit, when using the basic control on the VSM, for different values of H (a)(d) $H = 3\ s$, (b)(e) $H = 5\ s$, and (c)(f) $H = 7\ s$. (a),(b), and (c) show results when applying short circuit at 'Terminal(1)' and (d),(e), and (f) show results when applying short circuit at 'Terminal(2)'.

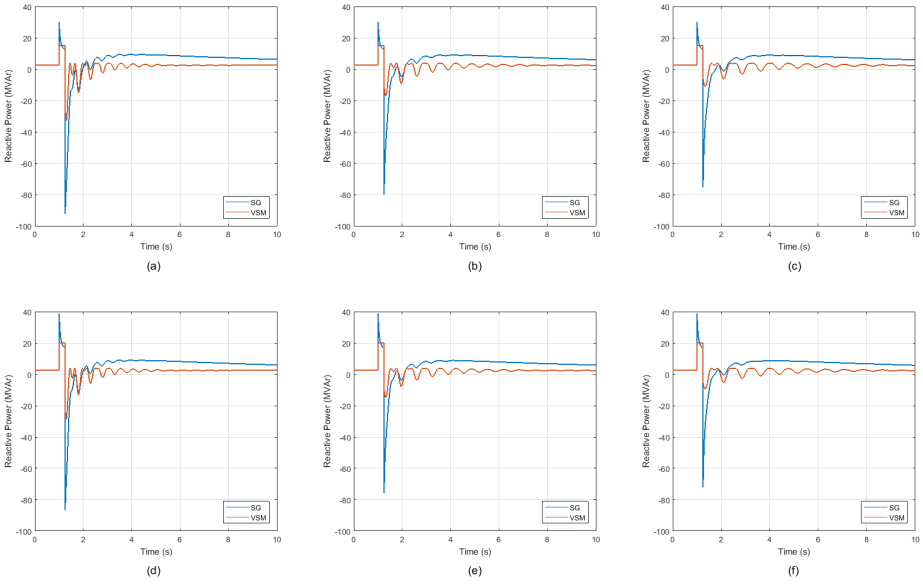

Figure 5.12: The reactive power output of the VSM and SG during short circuit, when using the basic control on the VSM, for different values of H (a)(d) $H = 3\ s$, (b)(e) $H = 5\ s$, and (c)(f) $H = 7\ s$. (a),(b), and (c) show results when applying short circuit at 'Terminal(1)' and (d),(e), and (f) show results when applying short circuit at 'Terminal(2)'.

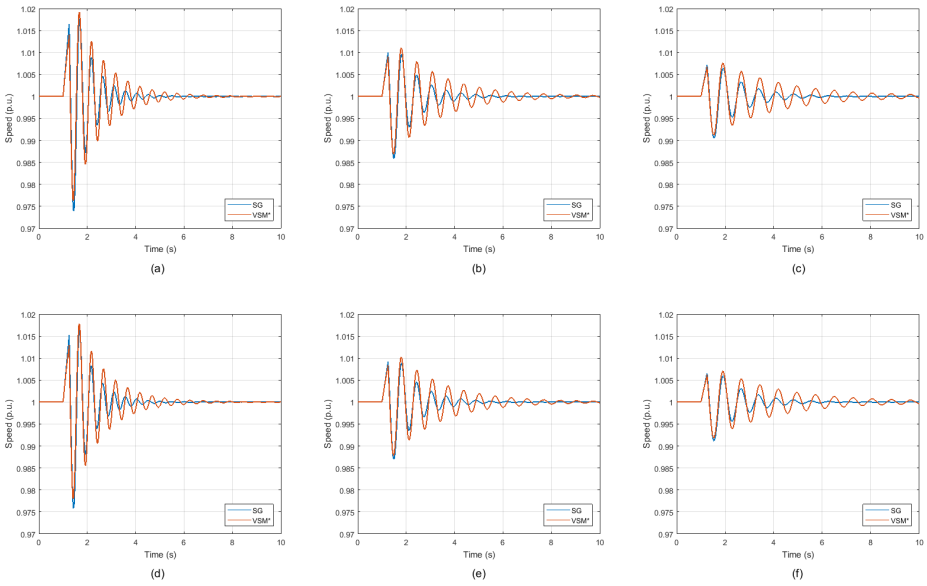

Figure 5.13: The rotor speed of the VSM and SG during short circuit, when using the basic control on the VSM, for different values of H (a)(d) $H = 3\ s$, (b)(e) $H = 5\ s$, and (c)(f) $H = 7\ s$. (a),(b), and (c) show results when applying short circuit at 'Terminal(1)' and (d),(e), and (f) show results when applying short circuit at 'Terminal(2)'.

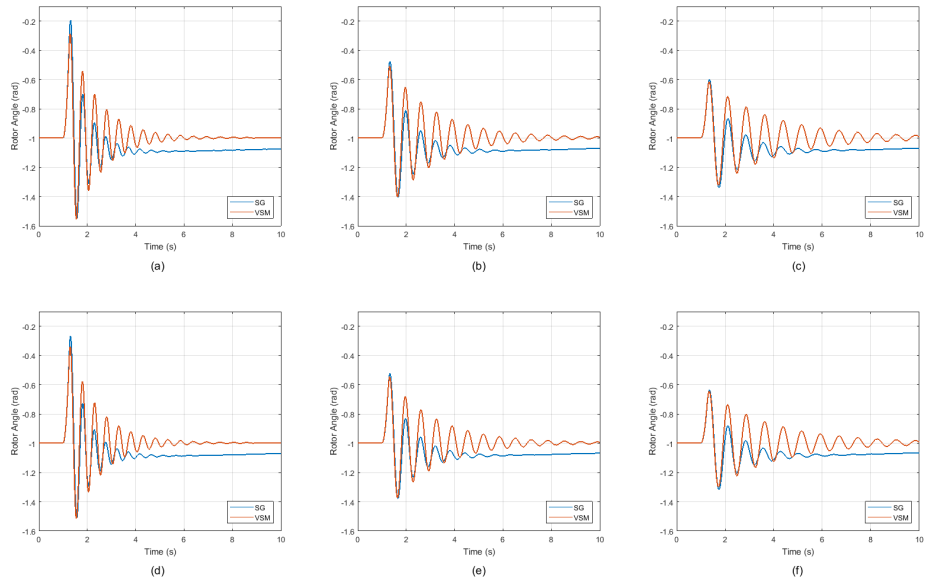

Figure 5.14: The rotor angle of the VSM and SG during short circuit, when using the basic control on the VSM, for different values of H (a)(d) $H = 3\ s$, (b)(e) $H = 5\ s$, and (c)(f) $H = 7\ s$. (a),(b), and (c) show results when applying short circuit at 'Terminal(1)' and (d),(e), and (f) show results when applying short circuit at 'Terminal(2)'.

5.2.2 VSM with current control

The main purpose of using this kind of fault is to test the functionality of the current controller in the VSM. Figure 5.16 demonstrate the ability of the VSM control to limit the current to 1 $p.u.$ for all the test scenarios. However, since the VSM control ultimately outputs voltage settings to converter, the only way to obtain the reduced current is to reduce the voltage and this can be seen in figure 5.15. Notice that the VSM voltage closely matched the SG when the current controller was not used, but that contributed to the high current observed at the previous test scenario. Furthermore, figure 5.17 and figure 5.18 show the active and reactive power plots, where the effect of saturating the current in the current control loop is clearly visible in the VSM signals. Moreover, adding an improved power reference and increasing the damping coefficient led to the results obtained in figure 5.19 and figure 5.20, which show the rotor speed and rotor angle respectively. It can be seen that the initial swing of the VSM's slip speed is reduced duo to decreasing P_{ref} during the faults and, also, having higher damping acting on the virtual rotor of the VSM. As a result, the virtual rotor angle was reduced, given that it is obtained by direct integration of the slip speed.

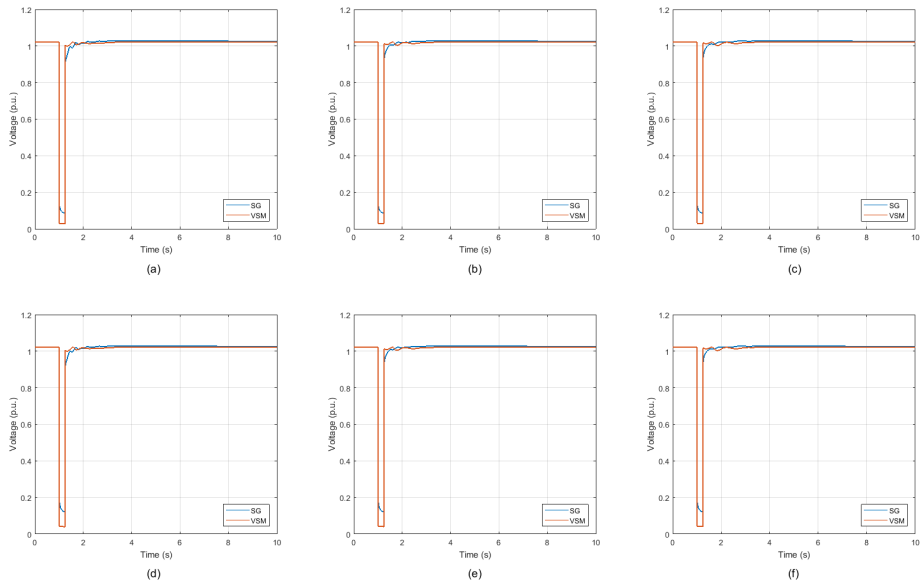

Figure 5.15: The voltage output of the VSM and SG during short circuit, when using the improved control on the VSM, for different values of H (a)(d) $H = 3\ s$, (b)(e) $H = 5\ s$, and (c)(f) $H = 7\ s$. (a),(b), and (c) show results when applying short circuit at 'Terminal(1)' and (d),(e), and (f) show results when applying short circuit at 'Terminal(2)'.

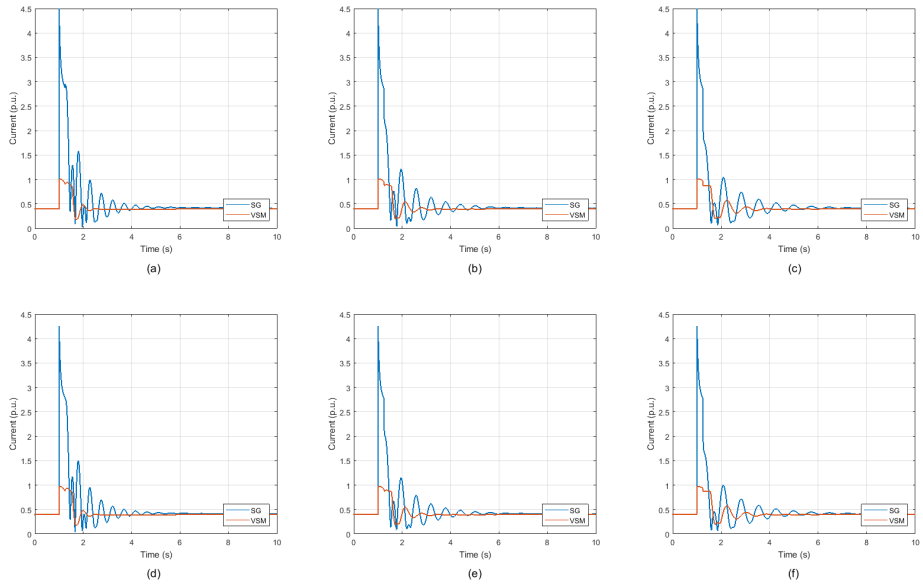

Figure 5.16: The current output of the VSM and SG during short circuit, when using the improved control on the VSM, for different values of H (a)(d) $H = 3\ s$, (b)(e) $H = 5\ s$, and (c)(f) $H = 7\ s$. (a),(b), and (c) show results when applying short circuit at 'Terminal(1)' and (d),(e), and (f) show results when applying short circuit at 'Terminal(2)'.

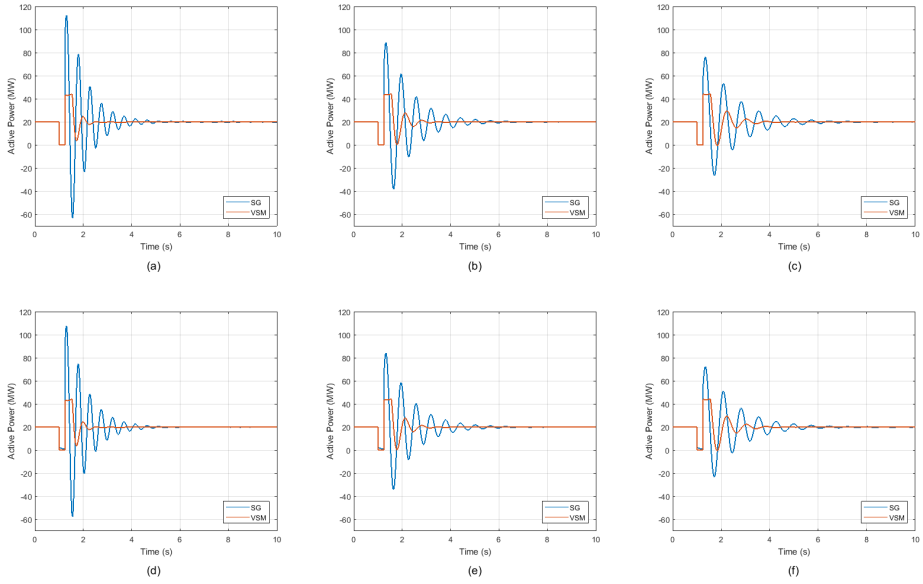

Figure 5.17: The active power output of the VSM and SG during short circuit, when using the improved control on the VSM, for different values of H (a)(d) $H = 3$ s , (b)(e) $H = 5\ s$, and (c)(f) $H = 7\ s$. (a),(b), and (c) show results when applying short circuit at 'Terminal(1)' and (d),(e), and (f) show results when applying short circuit at 'Terminal(2)'.

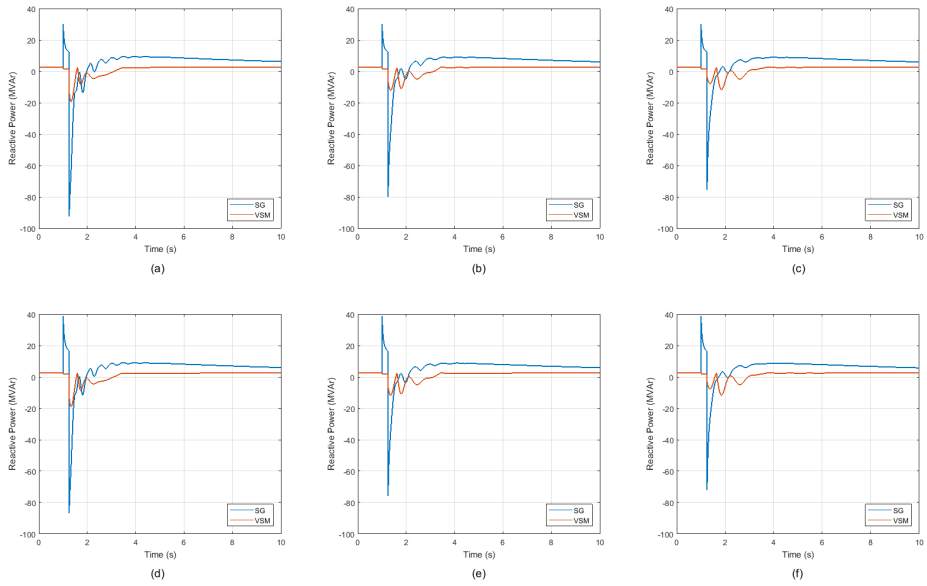

Figure 5.18: The reactive output of the VSM and SG during short circuit, when using the improved control on the VSM, for different values of H (a)(d) $H = 3\ s$, (b)(e) $H = 5\ s$, and (c)(f) $H = 7\ s$. (a),(b), and (c) show results when applying short circuit at 'Terminal(1)' and (d),(e), and (f) show results when applying short circuit at 'Terminal(2)'.

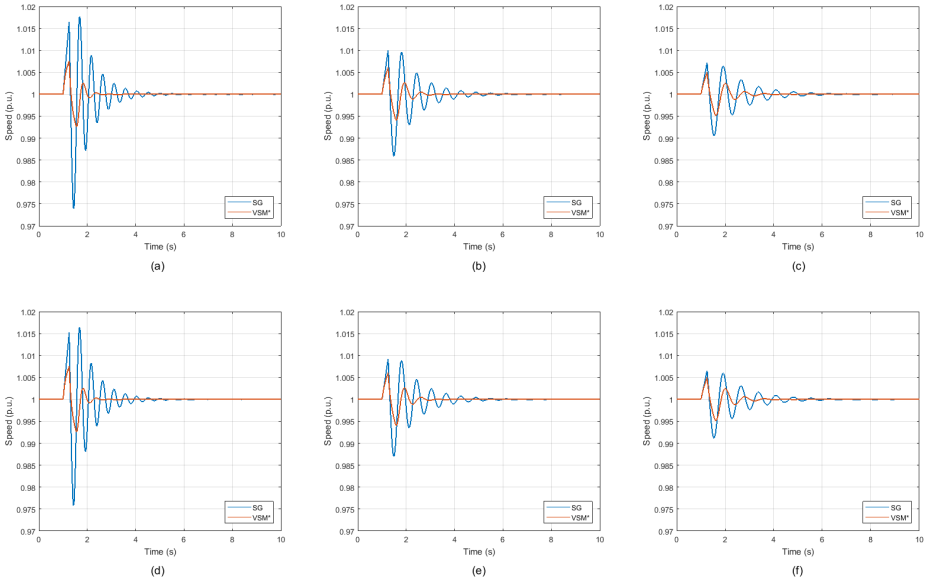

Figure 5.19: The rotor speed of the VSM and SG during short circuit, when using the improved control on the VSM, for different values of H (a)(d) $H = 3\ s$, (b)(e) $H = 5\ s$, and (c)(f) $H = 7\ s$. (a),(b), and (c) show results when applying short circuit at 'Terminal(1)' and (d),(e), and (f) show results when applying short circuit at 'Terminal(2)'.

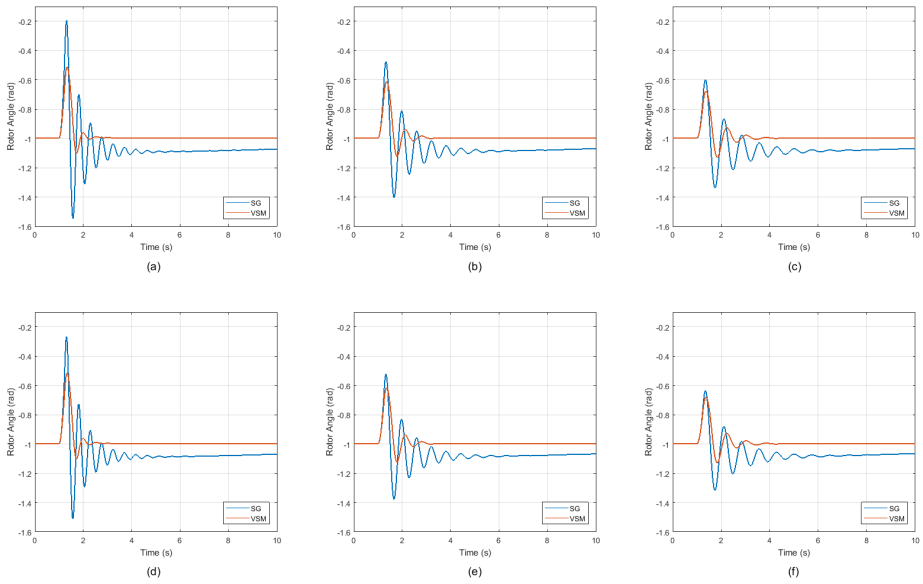

Figure 5.20: The rotor angle of the VSM and SG during short circuit, when using the improved control on the VSM, for different values of H (a)(d) $H = 3\ s$, (b)(e) $H = 5\ s$, and (c)(f) $H = 7\ s$. (a),(b), and (c) show results when applying short circuit at 'Terminal(1)' and (d),(e), and (f) show results when applying short circuit at 'Terminal(2)'.

5.3 VSM inertial response

During the simulation of load step events, the settling frequency is found to be 49.808 Hz and equation 2.3 was used to calculate the theoretical energy that should be injected to the system, as a result of the change in frequency. Then, the equation is written as

$$\Delta W_k = \frac{1}{2} J(\omega_{m0}^2 - \omega_{m1}^2), \tag{5.1}$$

where J is obtained using equation 2.4, for the different H values used in the simulation, and ω_{m0}^2 and ω_{m1}^2 are the nominal frequency and settling frequency, respectively. The energy can be calculated numerically from the power curves, obtained from the simulations, by integrating the area under the curve with 20 MW as reference. The results are compared to the theoretical values. Tables 5.1, 5.2, and 5.3 show the results obtained from the SG, the basic VSM control, and the improved VSM control, respectively.

Table 5.1: Comparison of energy injected with the SG.

$H\ (s)$	$W_k^{theoretical}\ (MWs)$	$W_k^{SG}\ (MWs)$	$\%\ error_{SG}$
3	1.1498	1.1642	1.252
5	1.9163	1.9345	0.950
7	2.6828	2.7259	1.607

Table 5.2: Comparison of energy injected with the basic VSM control.

$H\ (s)$	$W_k^{theoretical}\ (MWs)$	$W_k^{VSM}\ (MWs)$	$\%\ error_{VSM}$
3	1.1498	1.1466	0.278
5	1.9163	1.9143	0.104
7	2.6828	2.6827	0.004

Table 5.3: Comparison of energy injected with the modified VSM control.

$H\ (s)$	$W_k^{theoretical}\ (MWs)$	$W_k^{VSM}\ (MWs)$	$\%\ error_{VSM}$
3	1.1498	1.1478	0.174
5	1.9163	1.9184	0.110
7	2.6828	2.6894	0.246

Note that in the tables, the percentage error is calculated with the theoretical values taken as reference. It is observed that both VSM implementations result in very similar power injections to the theoretical values. Furthermore, the change in W_k between the two implementation is small due to having the modified control mainly working when there is a need for current limitation, otherwise, the synchronous machine emulation is the major contributing part in the control, which is the same as the basic control scheme. Moreover, in the load step simulations, current did not reach any alarming level, hence, the aforementioned conclusion was possible -refer to the Appendix A for a complete set of load step simulation results-.

6
Discussion

6.1 Analysis

Promising results were obtained from the VSM implementations in this report. In fact, the VSM exhibited better performance in some aspects like the reduction of frequency nadir, during load step case, when compared to a SG. This improvement was made possible by the addition of the inertia-dependant feedback KG. Moreover, it is found that by increasing KG, an even better frequency performance is obtained. However, it comes at the cost of requiring higher contribution from the ESS. Nonetheless, better results were delivered with less energy and closer matching to theoretical values, as it was shown in tables 5.1, 5.2, and 5.3. But the reason the addition of K_G was required remains unclear, since emulating a SG should be possible by modelling the swing equation without the need for a feedback. Another observation is the need for a time constant to be used in the slip speed integrator and removing it would result in a slow oscillatory behaviour that would take $1-2$ minutes to stabilize. This issue is observed when the VSM is subjected to short circuit faults. To remedy that, a selective control approach could be used, but then consideration of the delay to capture the fault type is necessary and further investigations are needed. Furthermore, VSM offered flexibility of control, since unlike a SG, the control parameters of a VSM are virtual and can be optimized to gain enhanced performance compared to SG. This can be realized, for example, by tuning the control parameter depending on the system condition, i.e. adding more inertial response from the VSM during critical system conditions. In addition, The inclusion of the current controller did not, heavily, affect the operation of the VSM, that is the VSM still emulates a general synchronous machine behaviour, as it was observed from the virtual angle signals in the short circuit study.

6.2 Sustainability aspects

With the advancement of technology to generate energy from environmentally friendly sources, many countries have the ability to supply their demand through RES. But one of the reasons this advancement is halted, is the risk when connecting a relatively large contribution of inertia-less generation. The development of VSM technology would make the domination of CCG possible, in which RES are a major part of. In addition, the current converters that are used to to connect RES can be used for the VSM technology, since it is a matter of control configuration. However, there is the addition of ESS that is vital for the VSM operation, which basically consist of bat-

teries, and may result in producing chemical waste. On the other hand, facilitating the inclusion of CCG would eventually lead to replacing current SG. This means a lot of scraps would be created that should be recycled, if possible. But replacing SG also means reducing greenhouse gases, which is beneficial from an environmental point of view.

7

Conclusion and Recommendations

This chapter summarizes the thesis work done and provide recommendation of future work to built upon this project

7.1 Conclusion

To summarize, The thesis started by motivating the study with background information and defined the objective and scope of the work. After that, supporting theory were presented in the second chapter for a better understanding of the basics that this project needed to implement the VSM control. Then, previous studies regarding the effects of high penetration of CCG were demonstrated along with some suggested mitigating approaches that could be taken. Also, papers regarding VSM technology were reviewed and and differences in implementations were elaborated. The fourth chapter explained the control philosophy and the work setup and procedure to conduct the study. Following that, the results were presented, in which successful synchronous machine emulation was obtained, in two different case studies. Finally, analysis of the thesis results and discussion of sustainability aspects were included in the sixth chapter.

7.2 Recommendations

- The study is conducted on a simple 3-bus system, which does not entirely reflect real system behaviour. Hence, the study should be done on more practical systems, e.g. Nordic 32.
- More research needs to be done to understand the underlying reason for the need of adding KG in the control; that is to obtain a more robust converter control scheme.
- Exploring the possibilities of improving the VSM technology to surpass conventional SG in terms stabilizing the power grid.
- The effects of controller delays were not considered in this thesis and should be investigated for practical implementation.
- ESS were not modelled in the converter and assumed availability of energy. Future work should include ESS models with rating based on system requirements and feasibility.
- Studying the effects of modelling governors in the VSM and how would it impact the system.
- Considering the effect of current limitation, in the VSM, on fault detection and how it can be resolved to avoid blinding over-current relays.

Bibliography

[1] H. Urdal, R. Ierna, J. Zhu, et al. "System strength considerations in a converter dominated power system". In: *IET Renewable Power Generation* 9.1 (2015), pp. 10–17. ISSN: 1752-1416. DOI: 10.1049/iet-rpg.2014.0199.

[2] Richard Ierna, Jiebei Zhu, Andrew J. Roscoe, et al. "Effects of VSM convertor control on penetration limits of non-synchronous generation in the GB power system". In: *15th Wind Integration Workshop*. This paper was presented at the 15th Wind Integration Workshop and published in the workshop's proceedings. Nov. 2016. URL: https://strathprints.strath.ac.uk/58052/.

[3] Prabha Kundur, Neal J Balu, and Mark G Lauby. *Power system stability and control*. Vol. 7. McGraw-hill New York, 1994.

[4] Joan Rocabert, Alvaro Luna, Frede Blaabjerg, et al. "Control of power converters in AC microgrids". In: *IEEE transactions on power electronics* 27.11 (2012), pp. 4734–4749.

[5] Frede Blaabjerg, Remus Teodorescu, Marco Liserre, et al. "Overview of control and grid synchronization for distributed power generation systems". In: *IEEE Transactions on industrial electronics* 53.5 (2006), pp. 1398–1409.

[6] Joonas Puukko, T Messo, and T Suntio. "Effect of photovoltaic generator on a typical VSI-based three-phase grid-connected photovoltaic inverter dynamics". In: (2011).

[7] Thanh Hai Nguyen and Dong-Choon Lee. "A novel current control scheme of grid converters for small PMSG wind turbines under grid voltage distortion". In: *Power Electronics and Machines in Wind Applications (PEMWA), 2012 IEEE*. IEEE. 2012, pp. 1–6.

[8] H. R. Chamorro, M. Ghandhari, and R. Eriksson. "Influence of the increasing non-synchronous generation on Small Signal Stability". In: *2014 IEEE PES General Meeting | Conference Exposition*. July 2014, pp. 1–5. DOI: 10.1109/PESGM.2014.6938796.

[9] G. Ivkovic. "Application of rate of change of frequency constraints for high wind penetration scenarios in a small power system". In: *2013 Australasian Universities Power Engineering Conference (AUPEC)*. Sept. 2013, pp. 1–5. DOI: 10.1109/AUPEC.2013.6725374.

[10] J. O'Sullivan, A. Rogers, D. Flynn, et al. "Studying the Maximum Instantaneous Non-Synchronous Generation in an Island System—Frequency Stability Challenges in Ireland". In: *IEEE Transactions on Power Systems* 29.6 (Nov. 2014), pp. 2943–2951. ISSN: 0885-8950. DOI: 10.1109/TPWRS.2014.2316974.

[11] W. Du, J. Bi, and H. F. Wang. "Small-signal angular stability of power system as affected by grid-connected variable speed wind generators- A survey of

recent representative works". In: *CSEE Journal of Power and Energy Systems* 3.3 (Sept. 2017), pp. 223–231. ISSN: 2096-0042. DOI: 10.17775/CSEEJPES.2016.00640.

[12] P. N. Papadopoulos and J. V. Milanović. "Impact of penetration of non-synchronous generators on power system dynamics". In: *2015 IEEE Eindhoven PowerTech*. June 2015, pp. 1–6. DOI: 10.1109/PTC.2015.7232308.

[13] K. Das, M. Altin, A. D. Hansen, et al. "Primary reserve studies for high wind power penetrated systems". In: *2015 IEEE Eindhoven PowerTech*. June 2015, pp. 1–6. DOI: 10.1109/PTC.2015.7232764.

[14] M. Nedd, C. Booth, and K. Bell. "Potential solutions to the challenges of low inertia power systems with a case study concerning synchronous condensers". In: *2017 52nd International Universities Power Engineering Conference (UPEC)*. Aug. 2017, pp. 1–6. DOI: 10.1109/UPEC.2017.8232001.

[15] Nahid-Al-Masood, N. Modi, and R. Yan. "Low inertia power systems: Frequency response challenges and a possible solution". In: *2016 Australasian Universities Power Engineering Conference (AUPEC)*. Sept. 2016, pp. 1–6. DOI: 10.1109/AUPEC.2016.7749335.

[16] H. Beck and R. Hesse. "Virtual synchronous machine". In: *2007 9th International Conference on Electrical Power Quality and Utilisation*. Oct. 2007, pp. 1–6. DOI: 10.1109/EPQU.2007.4424220.

[17] S. D'Arco, J. A. Suul, and O. B. Fosso. "Control system tuning and stability analysis of Virtual Synchronous Machines". In: *2013 IEEE Energy Conversion Congress and Exposition*. Sept. 2013, pp. 2664–2671. DOI: 10.1109/ECCE.2013.6647045.

[18] Salvatore D'Arco, Jon Are Suul, and Olav B. Fosso. "A Virtual Synchronous Machine implementation for distributed control of power converters in SmartGrids". In: *Electric Power Systems Research* 122 (2015), pp. 180–197. ISSN: 0378-7796. DOI: https://doi.org/10.1016/j.epsr.2015.01.001. URL: http://www.sciencedirect.com/science/article/pii/S0378779615000024.

[19] Hassan Bevrani, Toshifumi Ise, and Yushi Miura. "Virtual synchronous generators: A survey and new perspectives". In: *International Journal of Electrical Power Energy Systems* 54 (2014), pp. 244–254. ISSN: 0142-0615. DOI: https://doi.org/10.1016/j.ijepes.2013.07.009. URL: http://www.sciencedirect.com/science/article/pii/S0142061513003062.

[20] M. Yu, A. J. Roscoe, C. D. Booth, et al. "Use of an inertia-less Virtual Synchronous Machine within future power networks with high penetrations of converters". In: *2016 Power Systems Computation Conference (PSCC)*. June 2016, pp. 1–7. DOI: 10.1109/PSCC.2016.7540926.

[21] Y. Chen, R. Hesse, D. Turschner, et al. "Improving the grid power quality using virtual synchronous machines". In: *2011 International Conference on Power Engineering, Energy and Electrical Drives*. May 2011, pp. 1–6. DOI: 10.1109/PowerEng.2011.6036498.

[22] Andrew J Roscoe, Mengran Yu, Richard Ierna, et al. "A VSM (virtual synchronous machine) convertor control model suitable for RMS studies for resolving system operator/owner challenges". In: *15th Wind Integration Workshop*. This paper was presented at the 15th Wind Integration Workshop and pub-

lished in the workshop's proceedings. Nov. 2016. URL: https://strathprints.strath.ac.uk/58053/.

[23] M. A. Torres L., L. A. C. Lopes, L. A. Morán T., et al. "Self-Tuning Virtual Synchronous Machine: A Control Strategy for Energy Storage Systems to Support Dynamic Frequency Control". In: *IEEE Transactions on Energy Conversion* 29.4 (Dec. 2014), pp. 833–840. ISSN: 0885-8969. DOI: 10.1109/TEC.2014.2362577.

[24] L. Zhang, L. Harnefors, and H. Nee. "Power-Synchronization Control of Grid-Connected Voltage-Source Converters". In: *IEEE Transactions on Power Systems* 25.2 (May 2010), pp. 809–820. ISSN: 0885-8950. DOI: 10.1109/TPWRS.2009.2032231.

A

Appendix

A.1 Load step with basic VSM control

In the following plots, the results from conducting load step simulation on the SG and and the basic VSM implementation are shown. The load step is 25% load increase and is simulated for H values; 3 s, 5 s, and 7 s.

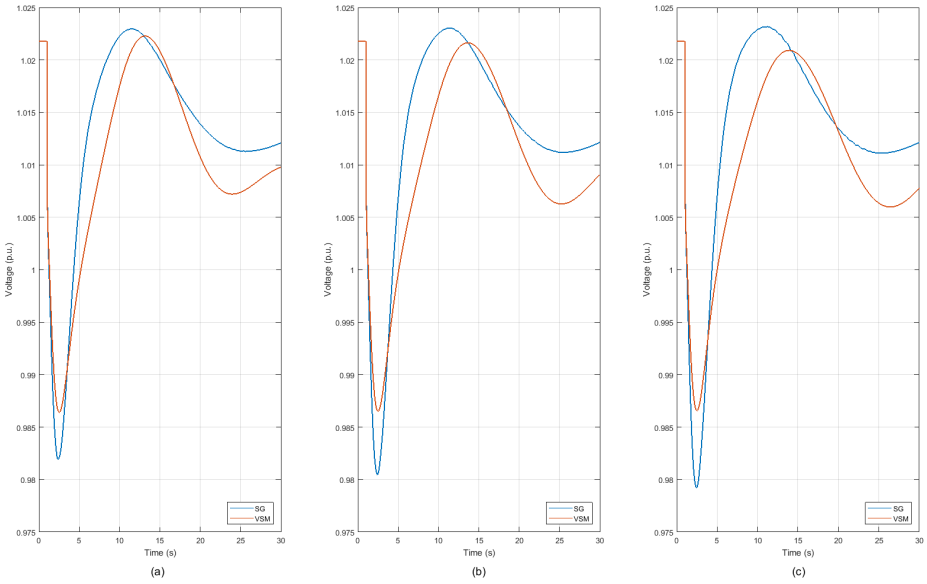

Figure A.1: The voltage output of the VSM and SG during load step, when using the basic control on the VSM, for different values of H (a) $H = 3s$, (b) $H = 5s$, and (c) $H = 7s$.

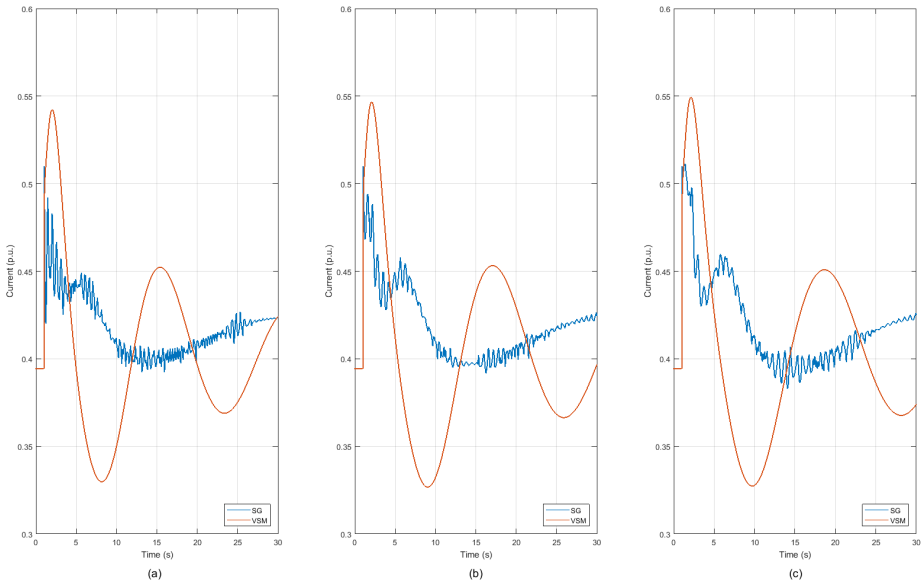

Figure A.2: The current output of the VSM and SG during load step, when using the basic control on the VSM, for different values of H (a) $H = 3s$, (b) $H = 5s$, and (c) $H = 7s$.

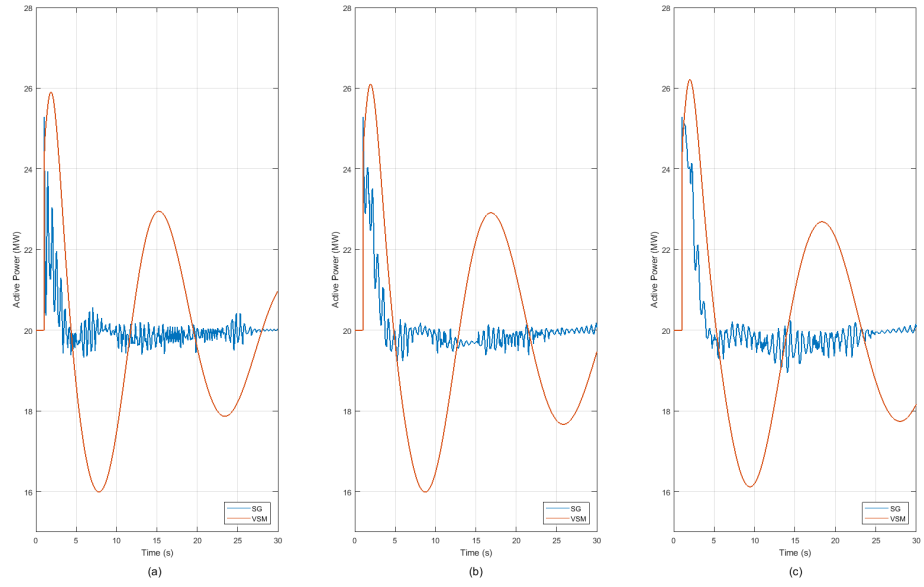

Figure A.3: The active power output of the VSM and SG during load step, when using the basic control on the VSM, for different values of H (a) $H = 3s$, (b) $H = 5s$, and (c) $H = 7s$.

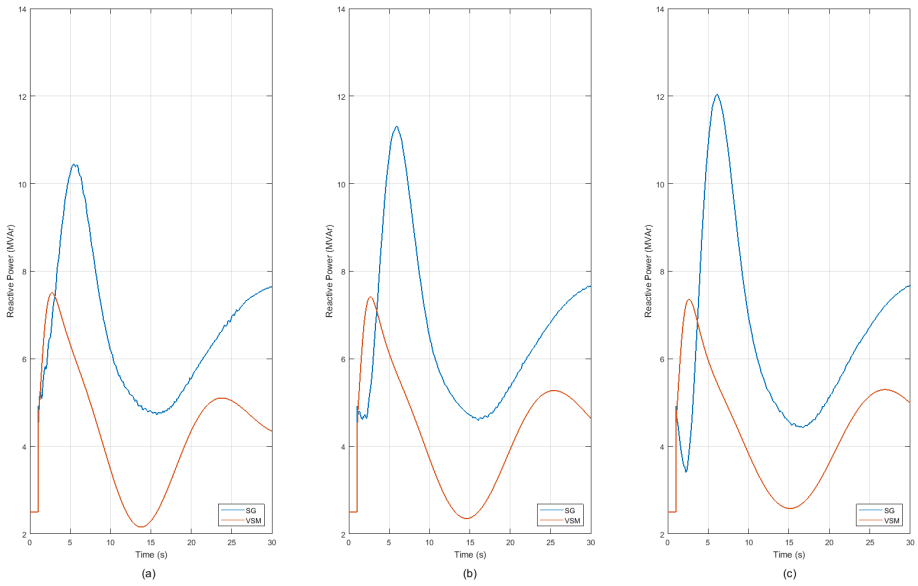

Figure A.4: The reactive power output of the VSM and SG during load step, when using the basic control on the VSM, for different values of H (a) $H = 3s$, (b) $H = 5s$, and (c) $H = 7s$.

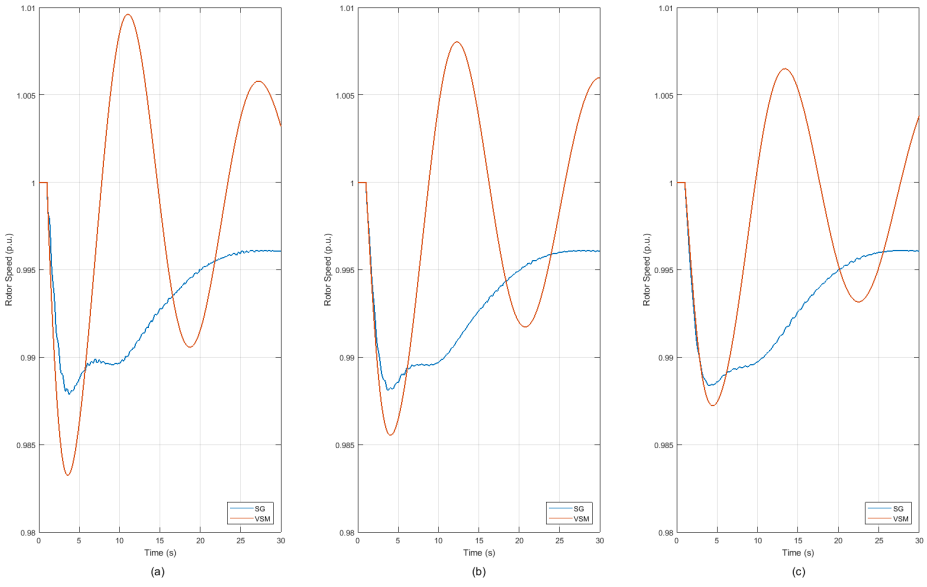

Figure A.5: The speed of the VSM and SG during load step, when using the basic control on the VSM, for different values of H (a) $H = 3s$, (b) $H = 5s$, and (c) $H = 7s$.

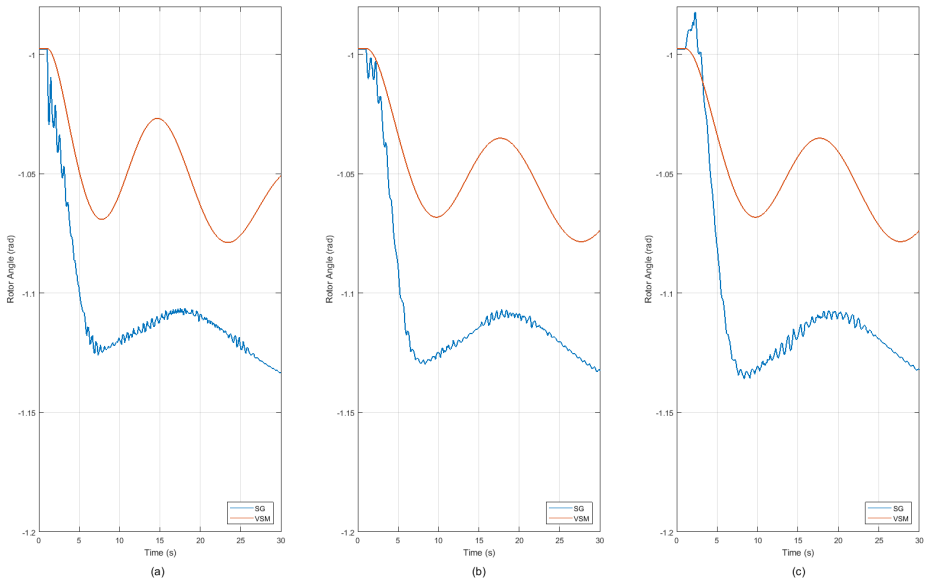

Figure A.6: The rotor angle of the VSM and SG during load step, when using the basic control on the VSM, for different values of H (a) $H = 3s$, (b) $H = 5s$, and (c) $H = 7s$.

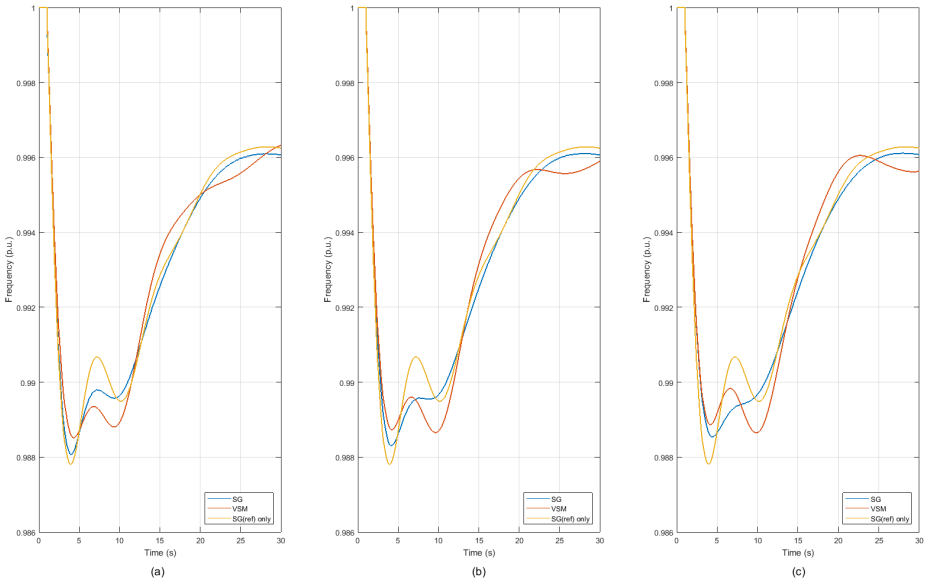

Figure A.7: The frequency at the bus where the VSM and SG are connected during load step, when using the basic control on the VSM, for different values of H (a) $H = 3s$, (b) $H = 5s$, and (c) $H = 7s$.

A.2 Load step with improved VSM control

In the below plots, the results from conducting load step simulation on the SG and and the improved VSM implementation are shown. The load step is 25% load increase and is simulated for H values; 3 s, 5 s, and 7 s.

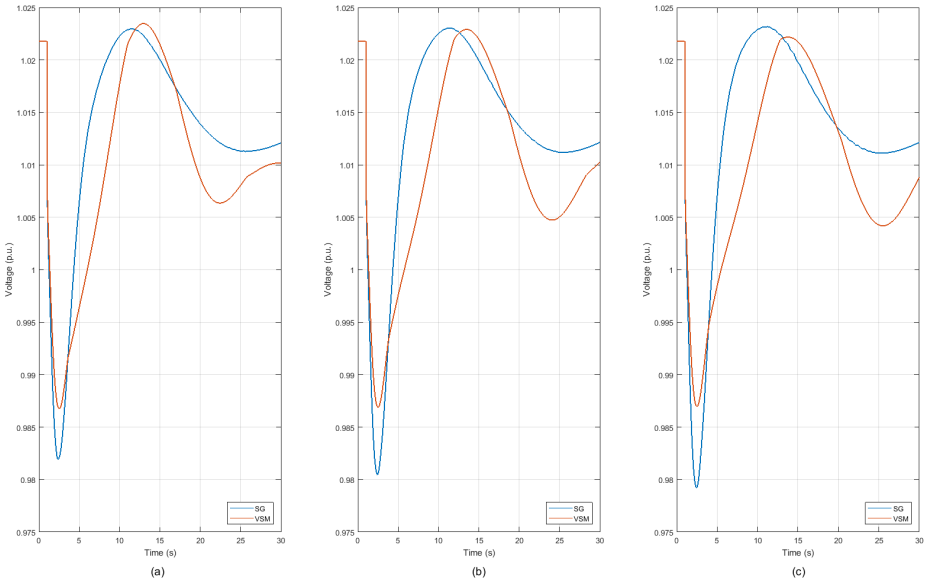

Figure A.8: The voltage output of the VSM and SG during load step, when using the improved control on the VSM, for different values of H (a) $H = 3s$, (b) $H = 5s$, and (c) $H = 7s$.

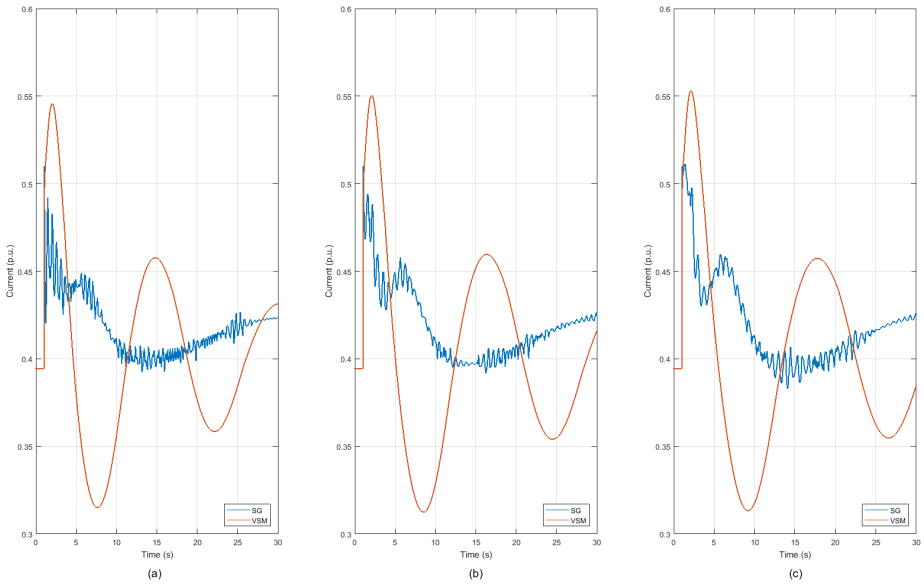

Figure A.9: The current output of the VSM and SG during load step, when using the improved control on the VSM, for different values of H (a) $H = 3s$, (b) $H = 5s$, and (c) $H = 7s$.

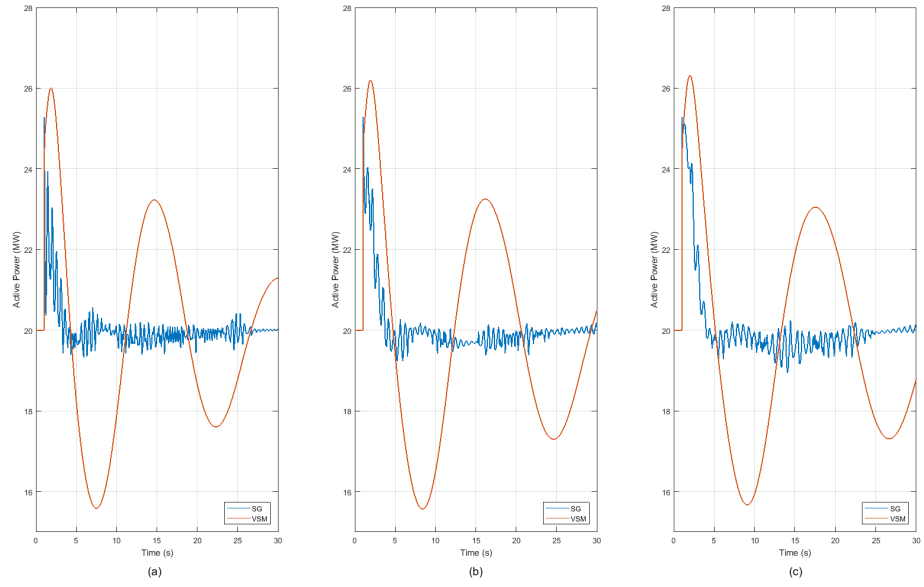

Figure A.10: The active power output of the VSM and SG during load step, when using the improved control on the VSM, for different values of H (a) $H = 3s$, (b) $H = 5s$, and (c) $H = 7s$.

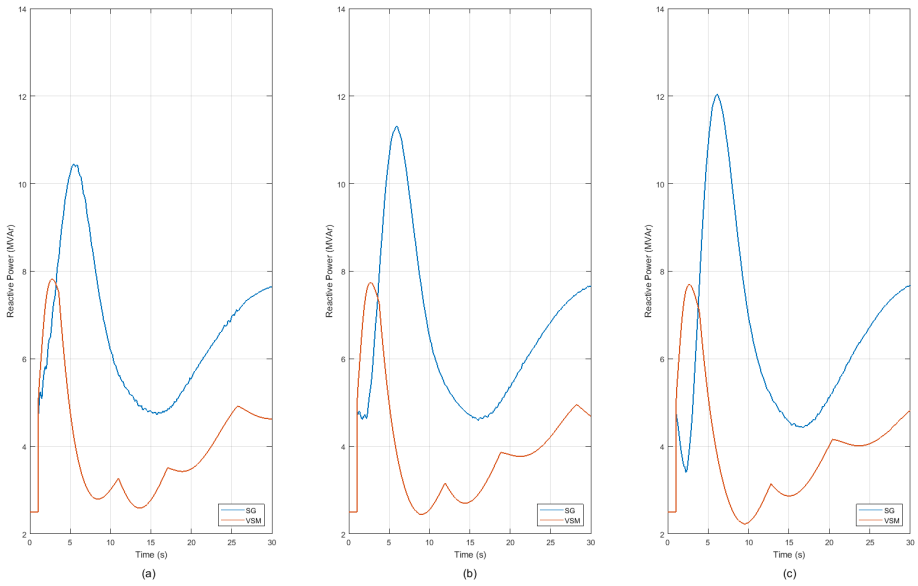

Figure A.11: The reactive power output of the VSM and SG during load step, when using the improved control on the VSM, for different values of H (a) $H = 3s$, (b) $H = 5s$, and (c) $H = 7s$.

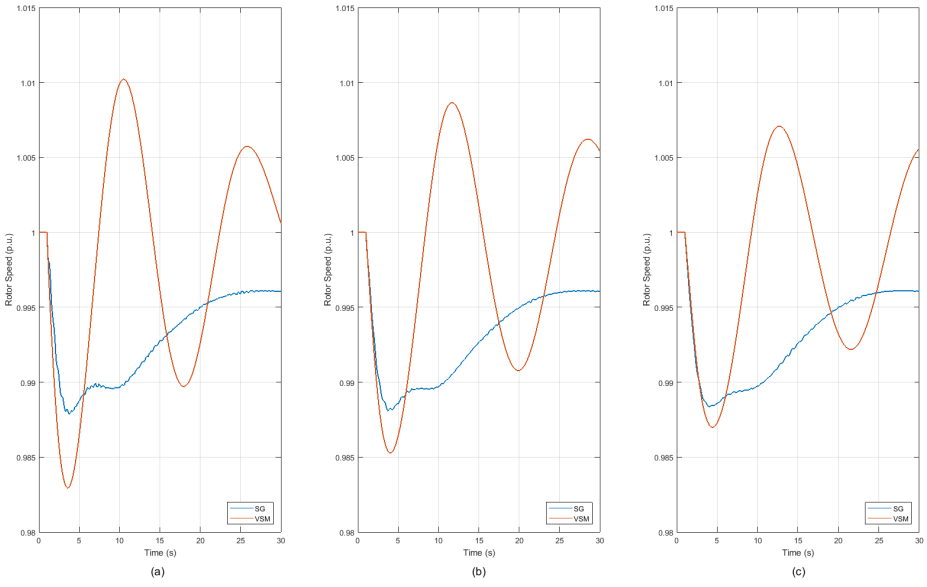

Figure A.12: The speed of the VSM and SG during load step, when using the improved control on the VSM, for different values of H (a) $H = 3s$, (b) $H = 5s$, and (c) $H = 7s$.

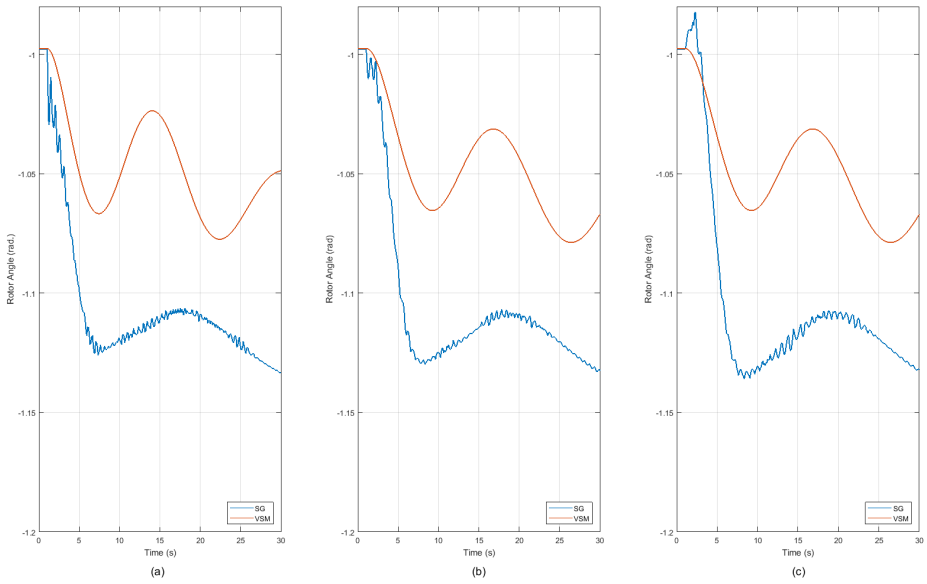

Figure A.13: The rotor angle of the VSM and SG during load step, when using the improved control on the VSM, for different values of H (a) $H = 3s$, (b) $H = 5s$, and (c) $H = 7s$.

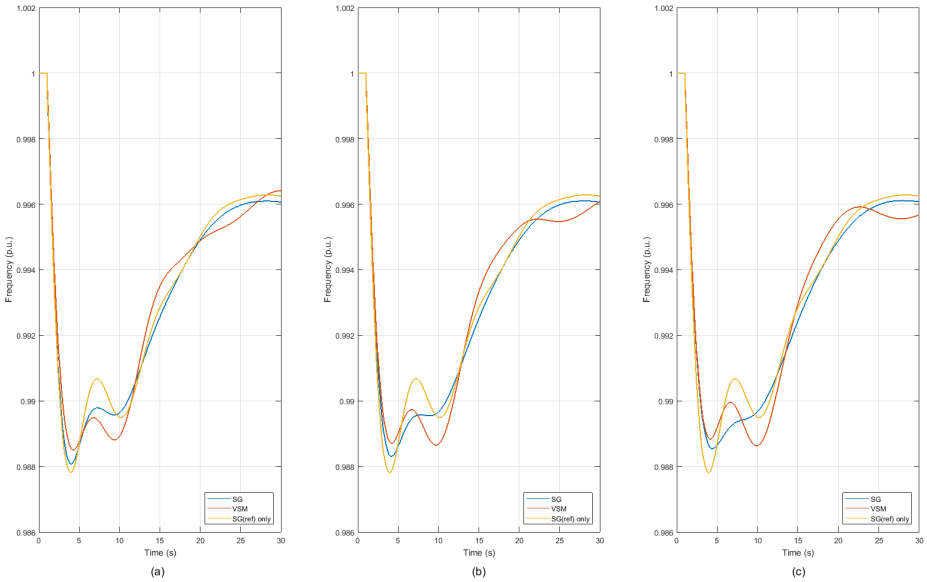

Figure A.14: The frequency at the bus where the VSM and SG are connected during load step, when using the improved control on the VSM, for different values of H (a) $H = 3s$, (b) $H = 5s$, and (c) $H = 7s$.